To the Graduate Council:

I am submitting herewith a thesis written by Hyo-In Park entitled "Rotational Structures near $40\hbar$ in ^{123}La." I have examined the final paper copy of this thesis for form and content and recommend that it be accepted in partial fulfillment of the requirements for the degree of Master of Science, with a major in Physics.

Leo L. Riedinger

Leo L. Riedinger, Major Professor

We have read this thesis
and recommend its acceptance:

Carrol Bingham

W. Nazarewicz

Accepted for the Council:

Vice Provost and Dean of Graduate Studies

Rotational Structures near 40 $\hbar$ in ^{123}La

A Thesis
Presented for the
Master of Science
Degree
The University of Tennessee, Knoxville

Hyo-In Park
May 2003

This thesis is dedicated
to everyone who makes me stand here.

ACKNOWLEDGEMENTS

It is very pleasure to express my deep appreciation to all members of nuclear structure group at the University of Tennessee. I have felt so fortunate to be the part of this wonderful group who makes me experience good reality everyday and provides the nice environment to do the research.

My sincere thanks go to Dr. Lee L. Riedinger for his generosity, encouragement, and inspiration. He has taught the long process of becoming a competent researcher as solving a labyrinth of the physics problems within the framwork of a big scientific picture. The wisdom he managed the schedule to conduct the research is admirable despite his heavy administrative responsibilities. I can never thank him enough. Thank you very much Dr. Riedinger!

I would like to extend my deepest thanks to Dr. Daryl J. Hartley. Without his enormous help and great patience, this work would not have been completed. I learned from him how to be thorough and how to prove what I know. He was always there to advise many research problems lucidly when I had difficulties. I also would like to thank Dr. Jing-Ye Zhang for his vigorous discussions to challenge me on the theoretical issues of this work.

Special thanks go to Dr. Ingemar Ragnarsson and Dr. Bao G. Dong for the theoretical calculations and many informative discussions. Their collaboration made it productive for me to understand how a theory applies to the experimental observable to extract the physical meaning. I would like to thank my committee members, Dr. Carrol Bingham and Dr. Witek Nazarewicz, for their careful review and advice on this thesis. I must thank Dr. Nazarewicz for giving me the theoretical intuition in nuclear physics from courses.

Equal thanks go to my friends who encourage me from a long distance. They are Young-Jae Chang, Woo-Jae Chang, Hyung-Gil Cho, Hyungmi Kim, Jin-Hyun Kim, Sun-Hee Kim, Eun-Hee Ko, Eun-Ae Ko, Hanna Im, Young-Eun Lee, Suk-Hyun Lim, Jin Kyoung Park. Especially, I would like to give my best thank to my roommate, Hyunjeong Kim. I will miss solving physics problems and having conversations about ethics, religion and life with you. Thank you for sharing part of your life with me.

I would like to express my infinite thanks to my family who has stood by me for my entire life. Thanks so much to my Dad and Mom for love, devotion, respect, and her fervent prayers. Thanks to Jung-Shik for your unconditional pray and care. Finally, I give all my gratitude and praise to the Lord who gave me the light in a world of darkness through the resurrection of Jesus Christ.

TABLE OF CONTENTS

CHAPTER PAGE

ABSTRACT

The neutron-deficient nucleus ^{123}La was studied via the ^{92}Mo(^{40}Ca,2ap) reaction at a beam energy of 184 MeV. Previously known bands were extended to much higher spin, and in two cases the structures are now observed near $40\hbar$. In addition, three new sequences were identified and linked into previously known bands. The lowest $(\pi, \alpha) = (+, -\frac{1}{2})$ structure displays similar characteristics to analogous bands in ^{127,129}La which have been suggested as examples of smooth band termination. Cranked Nilsson-Strutinsky calculations were compared with the experimental data in ^{123}La to determine whether this band is approaching a termination state as well.

LIST OF TABLES

LIST OF FIGURES

FIGURE **PAGE**

CHAPTER 1

INTRODUCTION

The atomic nucleus is one of most interesting quantal many-body systems in nature. It reveals many types of behavior which can be found individually in other systems, but which interact with one another in nuclei. The elementary nuclear excitations are regarded as a result of either single particle, vibrational, or collective motion. Single particle motions are described by nucleons moving independently in an average potential while macroscopic models like the liquid drop are based upon collective motions. One method to excite a nucleus is the fusion-evaporation reaction, which is ideal for populating very high angular momentum states ($I > 35$). In this reaction, accelerated projectile nuclei collide with a target nucleus, and the two fuse together to form a compound nucleus. The compound nucleus emits protons, neutrons, or alpha particles until it produces a highly excited residual nucleus. This residual nucleus does not want to remain in this excited state, rather it will decay towards the ground state by emission of γ rays. As the nucleus approaches the ground state, rotational structures, composed of sequential cascades of γ-rays, are observed in deformed nuclei. By examining these structures, many properties are deduced, such as the nuclear shape and the influence of nuclear pairing. The fusion evaporation reaction also provides an opportunity to access nuclei near the proton drip line when light beams and targets are used.

In an attempt to study nuclei near the proton drip line in the rare-earth region, we performed an experiment capitalizing on the sensitivity of Gammasphere and the selectivity of the Microball. As a result of this experiment, the decay schemes for some of the most neutron-deficient nuclei with $Z = 58 - 60$ [1, 2, 3, 4, 5] have been greatly extended over previous work (see Fig 1.1). The lightest La ($Z = 57$) nuclei with known excited states are ^{121,123}La [6, 7], and it has been nearly 15 years since

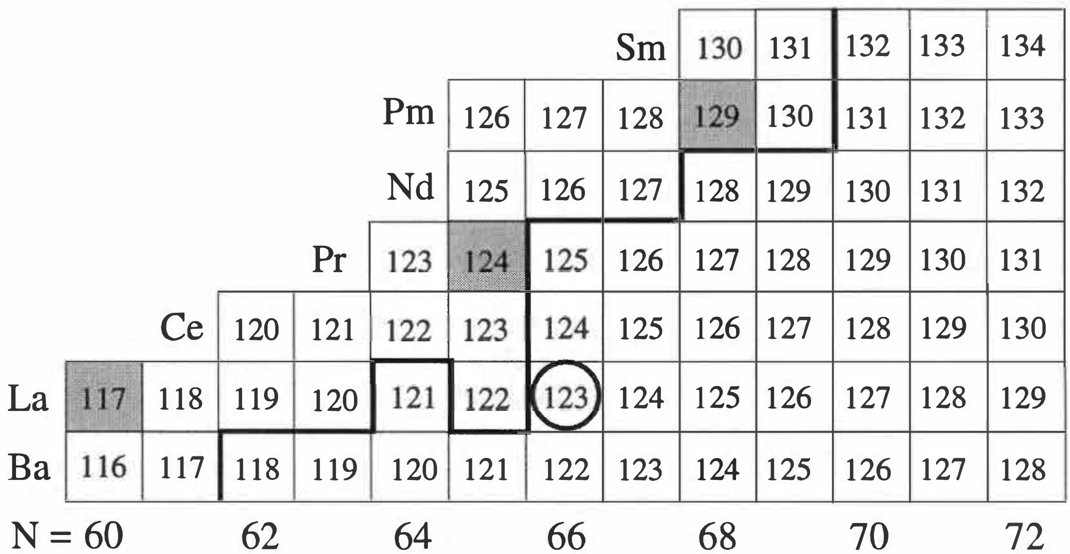

Figure 1.1: Chart of isotopes near the proton drip line in the $A \sim 130$ region. Nuclei to the right side of the dark line have known excited states. The shaded boxes indicate that a proton emitter has been identified (^{117}La [8] or the predicted proton drip line nuclei calculated by Vretnar *et al.* [9] (^{124}Pr and ^{129}Pm)). ^{123}La circled is discussed in this thesis.

either was studied. A weak reaction channel in our experiment was found to populate ^{123}La; however, these data nearly triple the number of observed states compared to the most recently published work [7].

The present investigation concentrates on the competition between collectivity and single particle motion at very high spins for the lowest $(\pi, \alpha) = (+, -\frac{1}{2})$ band in ^{123}La, elicited from comparing experimental observations with cranked Nilsson-Strutinsky calculations. Chapter 2 gives a brief description of the main experimental aspects such as population of high-spin states, γ-ray detection systems, and data analysis techniques. The theoretical background required for experimental data analysis and for the prediction of band termination is discussed in chapter 3. The experimental results and discussions are followed by conclusions.

CHAPTER 2

EXPERIMENTAL ASPECTS

2.1 Population of High-Spin States

In studies of high-spin states, it is necessary to find reactions which transfer the nucleus to the highest angular momentum with the largest cross section[1]. The fusion-evaporation reaction provides an efficient way to achieve this. The process of a fusion-evaporation reaction is schematically shown in Fig. 2.1. An incoming particle and the target nucleus fuse to form a compound nucleus in a highly excited state and with considerable angular momentum. The compound system first cools by evaporation of neutrons, protons, and α particles. Although the emission of particles reduces the energy of the system, they do not greatly decrease the angular momentum. Following particle evaporation, the revolving nucleus decays by γ-ray emission. This process removes the rest of the excitation energy and angular momentum from the system. Each initial state can decay to the ground state by many routes. No matter what the route is, these γ rays funnel down into a region near the yrast[2] line as shown in Fig. 2.2. This region involves discrete levels which form rotational bands built on a variety of states lying at low energies. Therefore, the information in terms of how the nuclear structure changes during the decay is obtained by measuring the properties of γ rays in cascades. The data which were analyzed for this thesis resulted from the bombardment of ^{40}Ca nuclei onto a target of ^{92}Mo. After the compound nucleus ^{132}Sm was formed and two α particles and one proton were emitted, the γ rays of ^{123}La were studied. In this experiment, over 15 different nuclei were populated and these nuclei are presented in Fig. 2.3. At one time, such result would have made this

[1]The cross-section is described by the yield in number of particles for a given interval of the particular reaction if the nucleus is bombarded with a flux of one projectile per area per interval.

[2]The yrast line is a sequence of all states that have the lowest energy for a given spin [10].

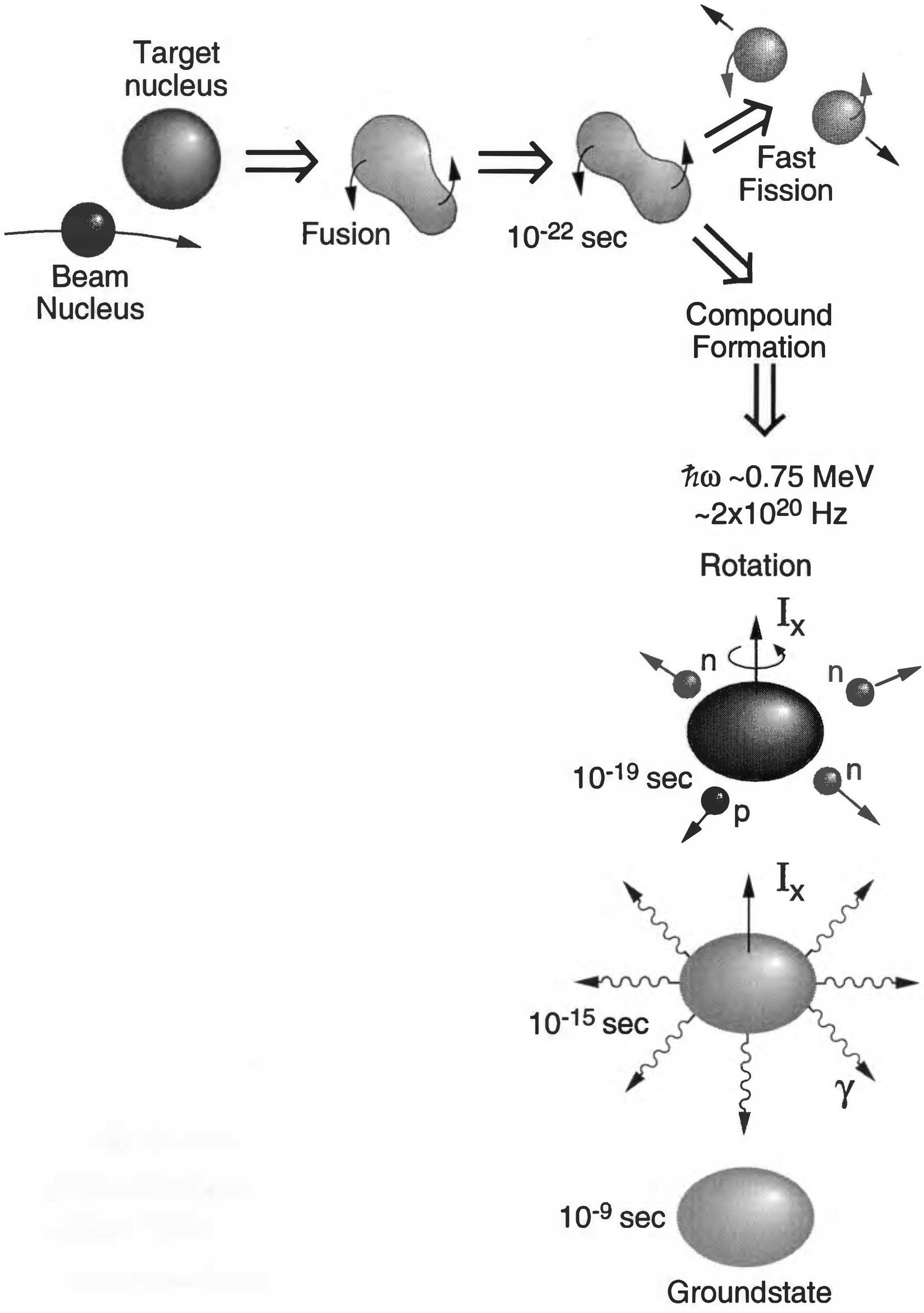

Figure 2.1: Schematic of a fusion-evaporation reaction.

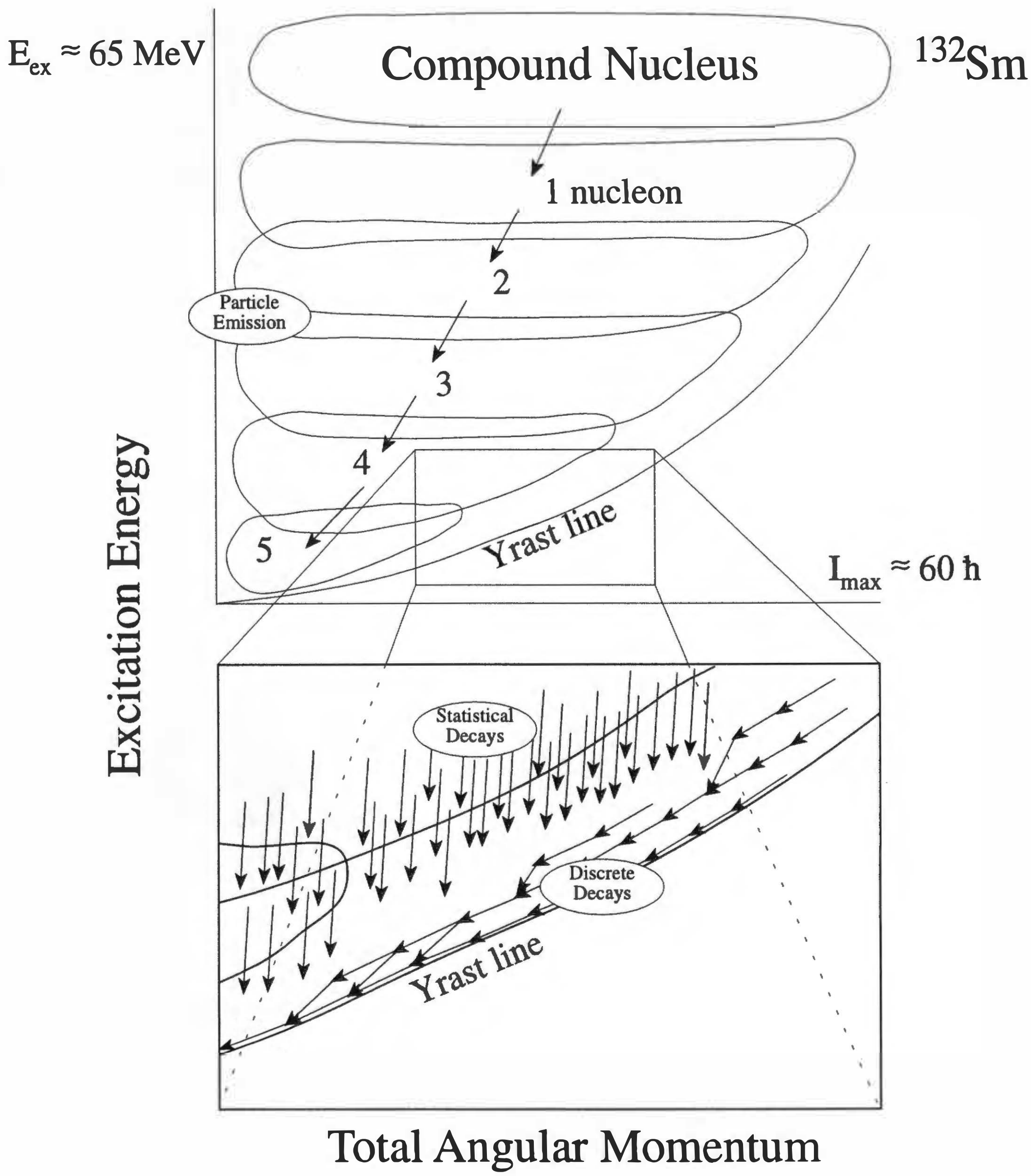

Figure 2.2: Excitation energy versus angular momentum illustration for the decay of a compound nucleus. The nuclear excitation is plotted as total angular momentum versus excitation energy. The labels "$E \sim 65$ MeV" and "$I \sim 60\hbar$" indicate the excitation energy and maximum angular momentum for a compound nucleus with $A \sim 130$, $A_i = 40$, and $A_t \sim 90$ [11].

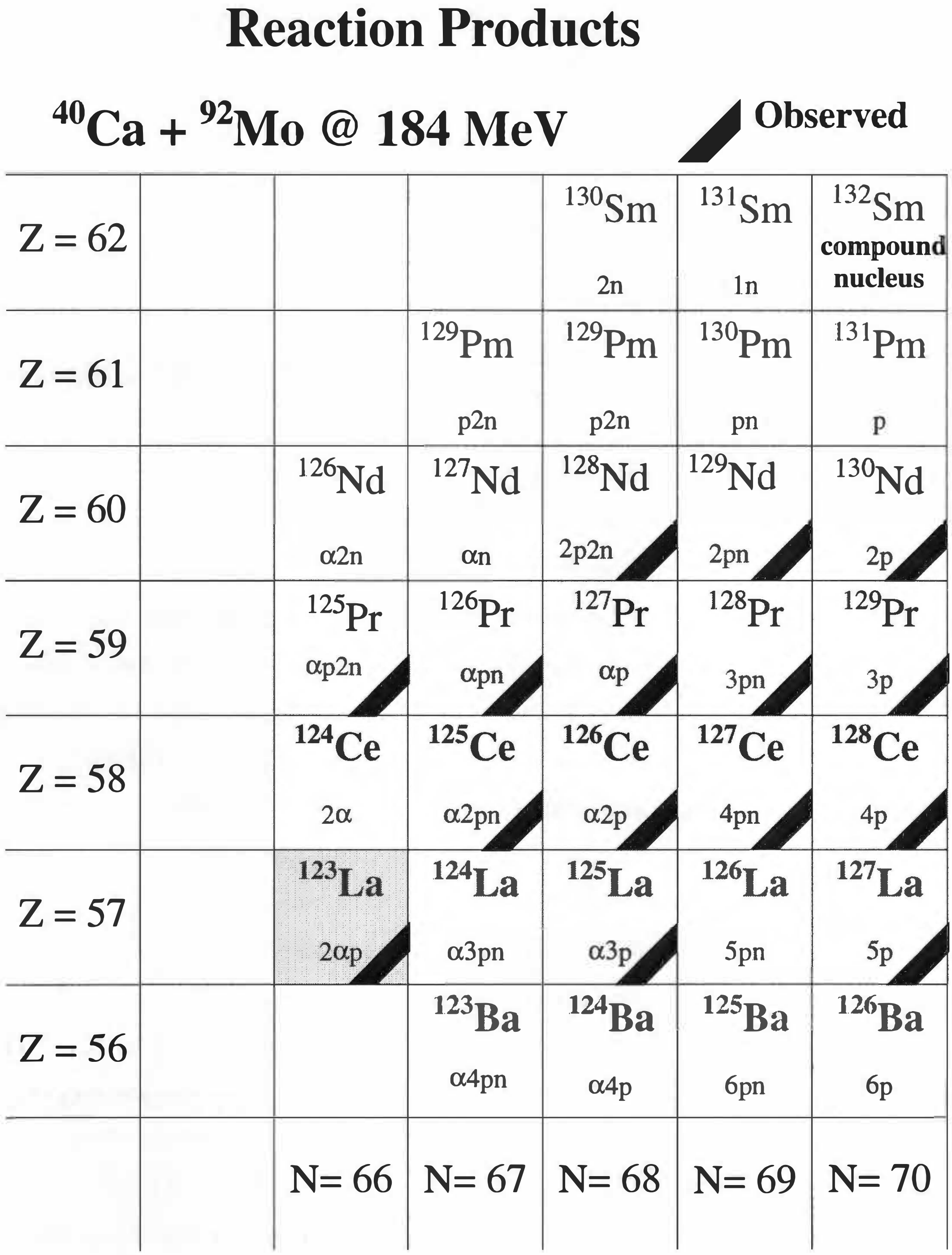

Figure 2.3: Map of the observed and populated nuclei following particle evaporation from ^{132}Sm compound nucleus.

reaction difficult to analyze. However, with the use of Microball and Gammasphere, it is an asset to separate the transitions from the different reaction channels and to study many nuclei from one experiment.

2.2 Experimental Device

2.2.1 Gammasphere Spectrometer

Gammasphere is a spectrometer of unparalleled detection efficiency and sensitivity to nuclear electromagnetic radiation. One of the key characteristics for Gammasphere is to have as much of the solid angle covered by as many Ge detectors as possible with a reasonably small solid angle covered by each detector. The combination of these features results in resolving extremely weak structures in reactions. The increasing probability of observing high-fold coincidences reduces background and the Doppler broadening effects are minimized by the small solid angle subtended by the individual detectors. Gammasphere has the capability of using 110 High-Purity Ge detectors (HPGe) of which 70 are segmented, each with a BGO shield. BGO ($Bi_4Ge_3O_{12}$) is a scintillation material in the form of a crystal. The high density of BGO and the large atomic number of the bismuth component provide the largest probability per unit volume of any scintillation material for the photoelectric absorption of γ rays. Thus, BGO is used as a shield material to detect the γ rays scattered out of the Ge crystals, which reduces the Compton continuum and improves the peak-to-total ratio[3]. The peak-to-total ratio obtained in Gammasphere is approximately 60% for ^{60}Co. The detectors are mounted at the following angles (in a forward-backward symmetry) with respect to the beam axis: 10 detectors at 17.3°, 10 at 31.7°, 10 at 37.4°, 20 at 50.1°, 10 at 58.3°, 20 at 69.8°, 10 at 79.2°, 10 at 80.7°, and 10 at 90.0°. The mechanical structure has two hemispheres with a diameter of 1.46 m, and a partial picture of Gammasphere with some of the possible 110 detectors installed is give in Fig. 2.4.

[3]The peak-to-total ratio is defined by the ratio of the full energy peak area to the total number of counts in the entire energy spectrum.

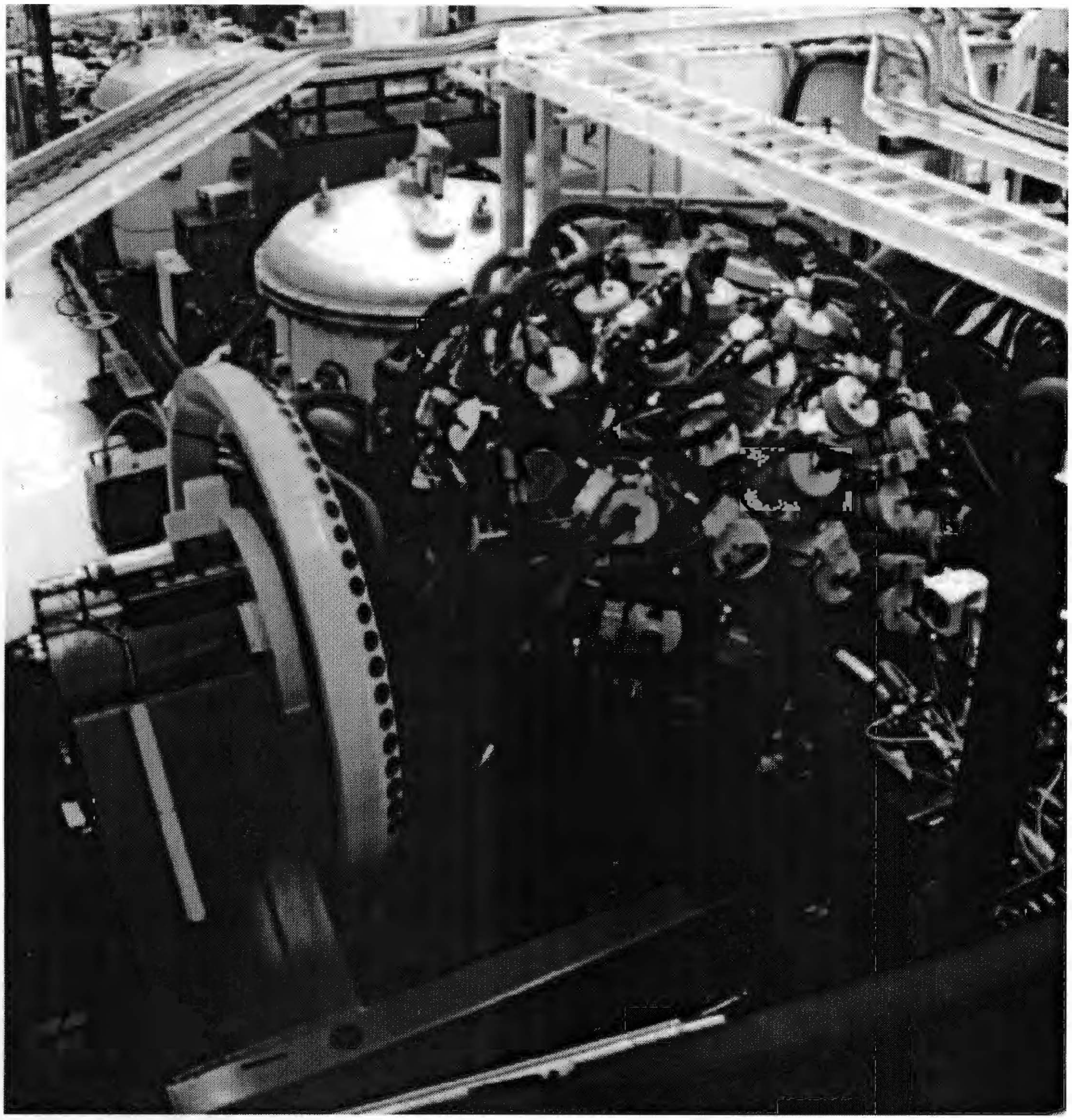

Figure 2.4: The Gammasphere spectrometer located at Argonne National Laboratory.

2.2.2 Microball Charged Particle Array

Although the neutron evaporation channels which are available to the compound nuclear system contribute to the reaction process in neutron-deficient nuclei of the mass 130 region, the probability for charged particle emission is high. In order to distinguish charged particles, we used the Microball detector array (Fig. 2.5), which is optimally designed to fit inside the Gammasphere scattering chamber. The device consists of 95 CsI scintillators closely packed to cover the angular range 4° - 172°, arranged in nine rings and has an overall solid angle coverage of 97%. Because of its small total mass, the degradation of the peak to total ratio of Gammasphere Ge detectors is minimized. Excellent gain stability with counting rate, temperature, and time is an important feature of Microball for obtaining good quality data. Fig. 2.6 shows the effect of using Microball to select the charged particle channel in our Gammasphere experiement. All γ events are tagged with charged-particle emissions detected by Microball. It allows us to greatly enhance the channel of interest leading to detailed study of several nuclei.

2.3 The γ-γ Coincidence Relationship: Level Scheme Construction

The method of γ-γ energy correlations becomes useful when the decay of a highly excited nucleus is complex and contains numerous levels. Since the decay is believed to proceed through various bands, measured correlations between two γ rays often correspond to transitions within the same rotational band. The simple decay scheme for a γ-γ correlation measurement is shown in Fig. 2.7. Each level has a lifetime (τ) which is shorter than the coincidence gate used for the detectors in coincidence. By choosing a time window ($t_w \approx 80ns$) greater than τ for the middle level, two detectors located at different angles θ_1 and θ_2 observe γ_1 to be in coincidence with γ_2 and γ_3. Since γ_2 and γ_3 are not correlated, no coincidence is observed except in random coincidences (*i.e.* background).

The coincidence data taken from Gammasphere can be analyzed by a cor-

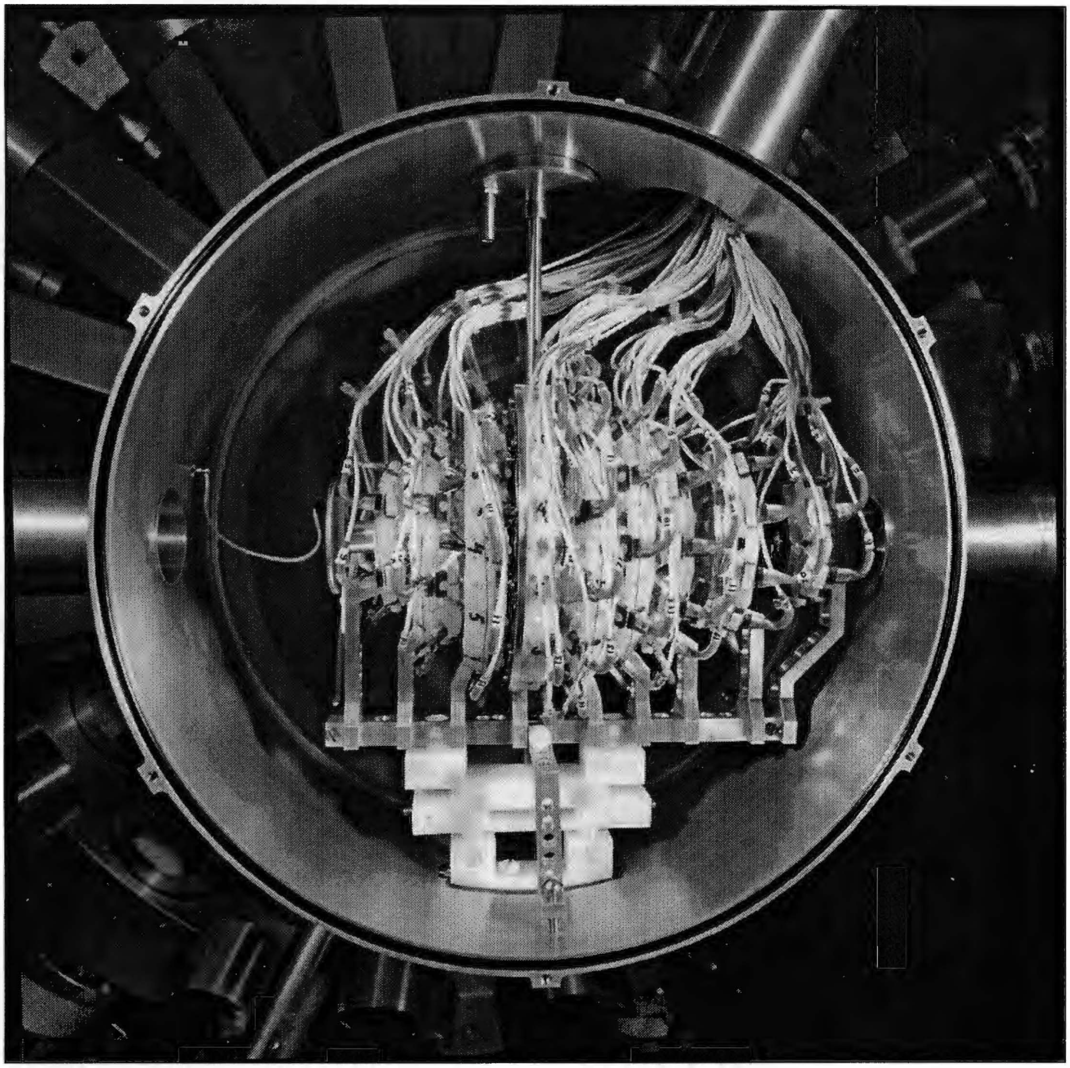

Figure 2.5: The Washington University Microball charged particle array.

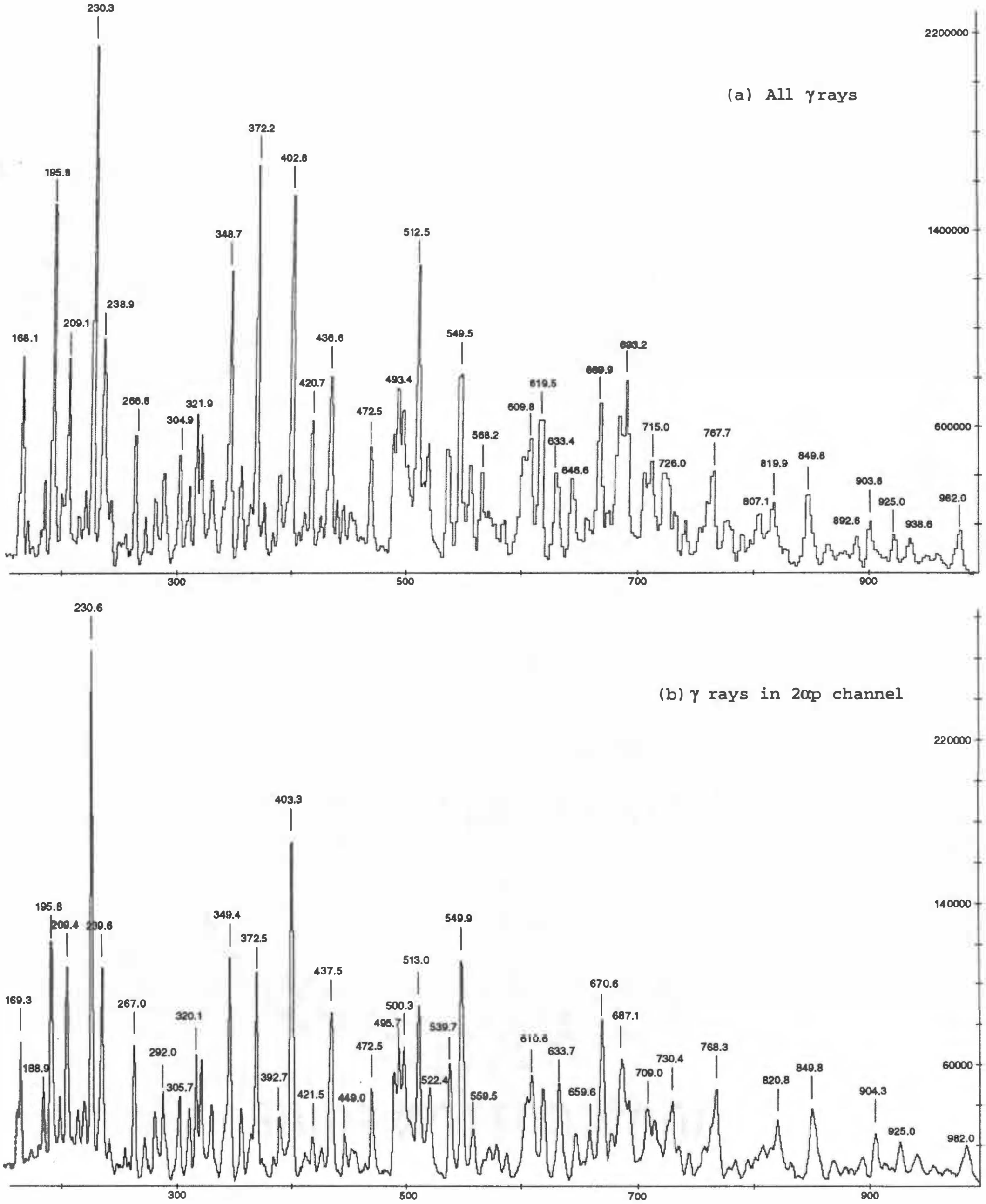

Figure 2.6: Spectra of the total γ-ray projection for all channels and the total projection of the $2\alpha p$ channel leading to ^{123}La, showing the sensitivity of charged-particle selection by the Microball.

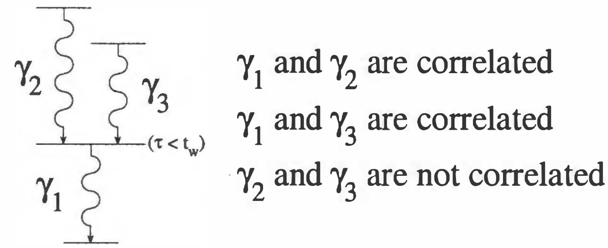

Figure 2.7: Simple decay scheme illustrating correlated γ rays.

relation matrix which is obtained from each pair of detectors in the experiment. The two coordinates of the matrix represent the γ-ray energies in the two detectors. Each point in the matrix corresponds to a measured coincidence between two detectors; the γ-γ correlation is symmetrical with respect to the 45° diagonal. The matrix exhibits a regular structure of ridges. The first ridge on each side of the diagonal corresponds to adjacent transitions in all participating cascades, the next ridge to transitions further apart, and so on. Thus, the distances between adjacent ridges are equivalent to the difference of adjacent γ rays in the cascades.

Based on an $E_\gamma \times E_\gamma \times E_\gamma$ cube for the analysis of γ-γ-γ coinncidence, the program called LEVIT8R [12] was used in this investigation. LEVIT8R enables the user to automatically inspect background-subtracted gated spectra in a simple, user friendly environment. The matrices are examined by taking "gates," that is, selecting a γ-ray energy on two of the axes and examining the projection of the coincidence γ rays on the third axis called double-gating. From these gates, the coincidence relationship between γ rays, which results from the nuclear decay to the ground state, can be determined. LEVIT8R allows one to determine the energies and intensities of the γ rays in the level scheme. These quantities play major roles to acquire the physical information about nuclear structure at high spin. It should be noted that the selectivity of double-gating, compared with single-gating, resolves doublet transitions where two γ rays have the same energy.

CHAPTER 3

Theoretical Background

Since there exists no unified model which describes the characteristics of all known nuclear phenomena, various theoretical models are introduced to examine particular aspects of nuclear phenomena. A qualitative description of deformed rotating nuclei is emphasized in this chapter, especially for the study of axially deformed nucleus ^{123}La. The Cranked Shell Model (CSM) has proven to be successful in interpreting the collective rotational bands at high angular momenta in terms of independent quasiparticles. Several experimental properties are compared with CSM predictions in chapter 4. A theoretical point of view on the non-collective nature of high-spin states is presented to compare band termination with experimental results in chapter 5.

3.1 Nuclear Shapes

A variety of different shapes has been predicted and observed depending on the ratio of protons to neutrons, conditions of excitation energy, or the spin of nuclei [13]. Deformed nuclei can be categorized by these shapes; prolate (two semi-minor axes equal), oblate (two semi-major axes equal), and triaxial (all three principal axes are different), according to the relative axis values of the ellipsoid as shown in Fig. 3.1. A nuclear shape can be parameterized by expansion of the radial vector, R, in terms of the spherical harmonic function,

$$R(\theta,\phi) = R_0\left[1+\alpha_{00}+\sum_{\lambda=0}^{\infty}\sum_{\mu=-\lambda}^{\lambda}\alpha_{\lambda\mu}Y_{\lambda\mu}(\theta,\phi)\right], \tag{3.1}$$

where R_0 is the radius of a sphere with the same volume as the parameterized shape. The condition that the nuclear volume stays constant for all deformations determines

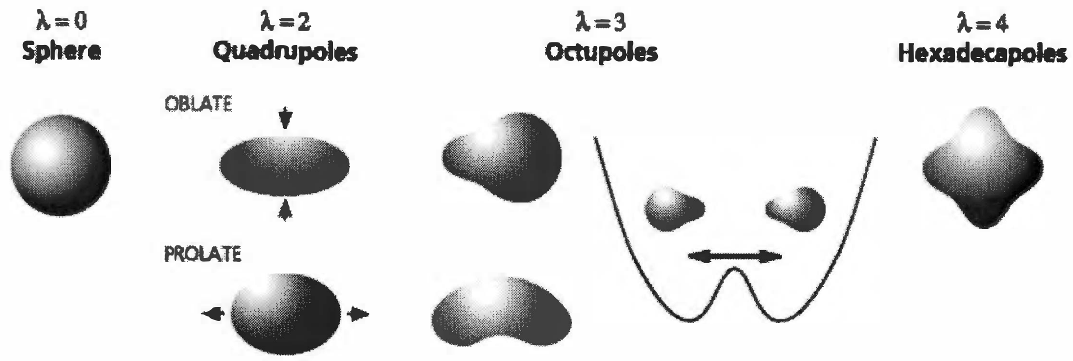

Figure 3.1: Nuclear shapes parameterized by spherical harmonic functions. Reproduced from [13].

the α_{00} parameter. The constant $\alpha_{\lambda\mu}$ is fixed by the requirement that the origin is in coincidence with the center of mass. Terms which include λ characterize the different orders of the corresponding distributions. For the nuclear surface in the $\lambda = 2$ order, the radial vector can be expressed as

$$R(\theta, \phi) = R_0 \left[1 + \alpha_{00} + \alpha_{20} Y_{20}(\theta', \phi') + 2\alpha_{22} Y_{22}(\theta', \phi')\right] \tag{3.2}$$

where

$$\alpha_{20} = \beta_2 \cos\gamma \tag{3.3}$$

and

$$\alpha_{22} = -\frac{1}{\sqrt{2}} \beta_2 \sin\gamma. \tag{3.4}$$

Thus, deformation parameters β_2 and γ represent axial stretching and the degree of triaxiality. Fig. 3.2 illustrates nuclear shapes described by β_2 and γ. Prolate deformation is expected if $\gamma = 0°$ and $\beta_2 \neq 0$ while oblate shapes are presented by $\gamma = \pm 60°$. Triaxial shapes are described by γ values between 0° and 60°. The values $\beta_2 = \gamma = 0$ correspond to spherical nuclei.

3.2 Deformed Shell Model: Nilsson Model

It was an important step in our understanding of the atomic nucleus when M. Mayer and H. Jensen independently proposed the development of a nuclear shell model for spherical nuclei, which correctly predicted the nuclear magic numbers. However, only

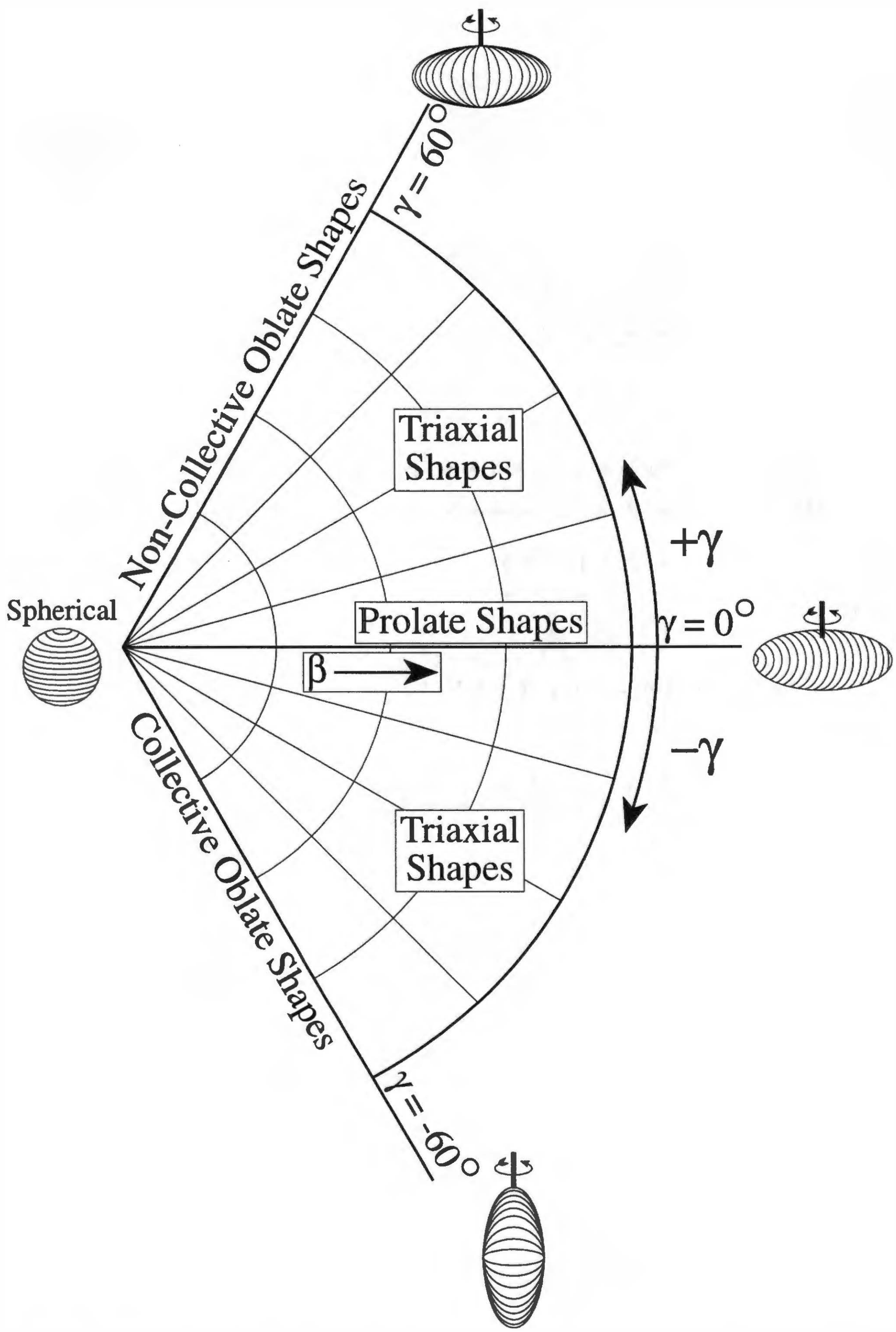

Figure 3.2: Nuclear shapes in relation to β_2 and γ are displayed in polar coordinates. Reproduced from Ref. [14].

a small fraction of nuclei are observed to be spherical. Nilsson considered the single-particle energy levels of all nucleons moving in an axially deformed harmonic oscillator potential [15, 16] giving a Hamiltonian of the form

$$H = \frac{\mathbf{p^2}}{2m} + \frac{1}{2}m\left[{\omega_x}^2(x^2+y^2)+{\omega_z}^2z^2\right] + C\mathbf{l}\cdot\mathbf{s} + D\mathbf{l^2}. \tag{3.5}$$

The first term is the kinetic energy of particle, and the second term represents the harmonic oscillator potential where ω_x, ω_y, and ω_z are the one-dimensional oscillator frequencies ($\omega_x = \omega_y$) in the x, y, and z directions [17]. The Nilsson Hamiltonian contains the spin-orbit term which produces the correct magic number and l^2 term to make the potential well more like a deformed square well, which is a better approximation to the nuclear potential well [17]. The Dl^2 term produces a splitting between levels with different values of l. This simulates the transitions from an oscillator potential, in which all l values within a major shell are degenerate, to a square well potential in which higher l levels in a major shell are more bounded than the lower l levels. The exact values of C and D are fixed to reproduce the observed level order and splitting near magic numbers at zero deformations, and may vary in going from one nucleus to another.

A Nilsson diagram is shown in Fig. 3.3, which shows the predicted energy levels as a function of nuclear deformation parameter ϵ_2. The order of the levels, indicated at $\epsilon_2 = 0$ (which defines a spherical shape) of Fig. 3.3 is simply the results of the shell model. Shells are labeled with the letters s, p, d, f,... (similar to the atomic shells) which have $l = 0, 1, 2, 3, ...$ and the total angular momentum is $j = l+s$. It is customary to use the following set of the asymptotic quantum numbers that are good at $\epsilon_2 \approx 0$

$$[Nn_z|\Lambda|]\,\Omega^{(\pi)} \tag{3.6}$$

where $N = n_z+n_\perp$ is the total oscillator quantum number, n_z is the number of quanta in oscillations (phonons) along the symmetry axis z, $n_\perp = n_x + n_y$ is the number of oscillator quanta perpendicular to the symmetry axis, $\Omega = \Lambda + \Sigma$ is the component of total angular momentum along the symmetry axis (Σ is the component of spin along the symmetry axis, $\pm\frac{1}{2}$), and $\Lambda = \pm n_\perp, \pm(n_\perp - 1), \ldots, \pm 1,$ or 0 is the component

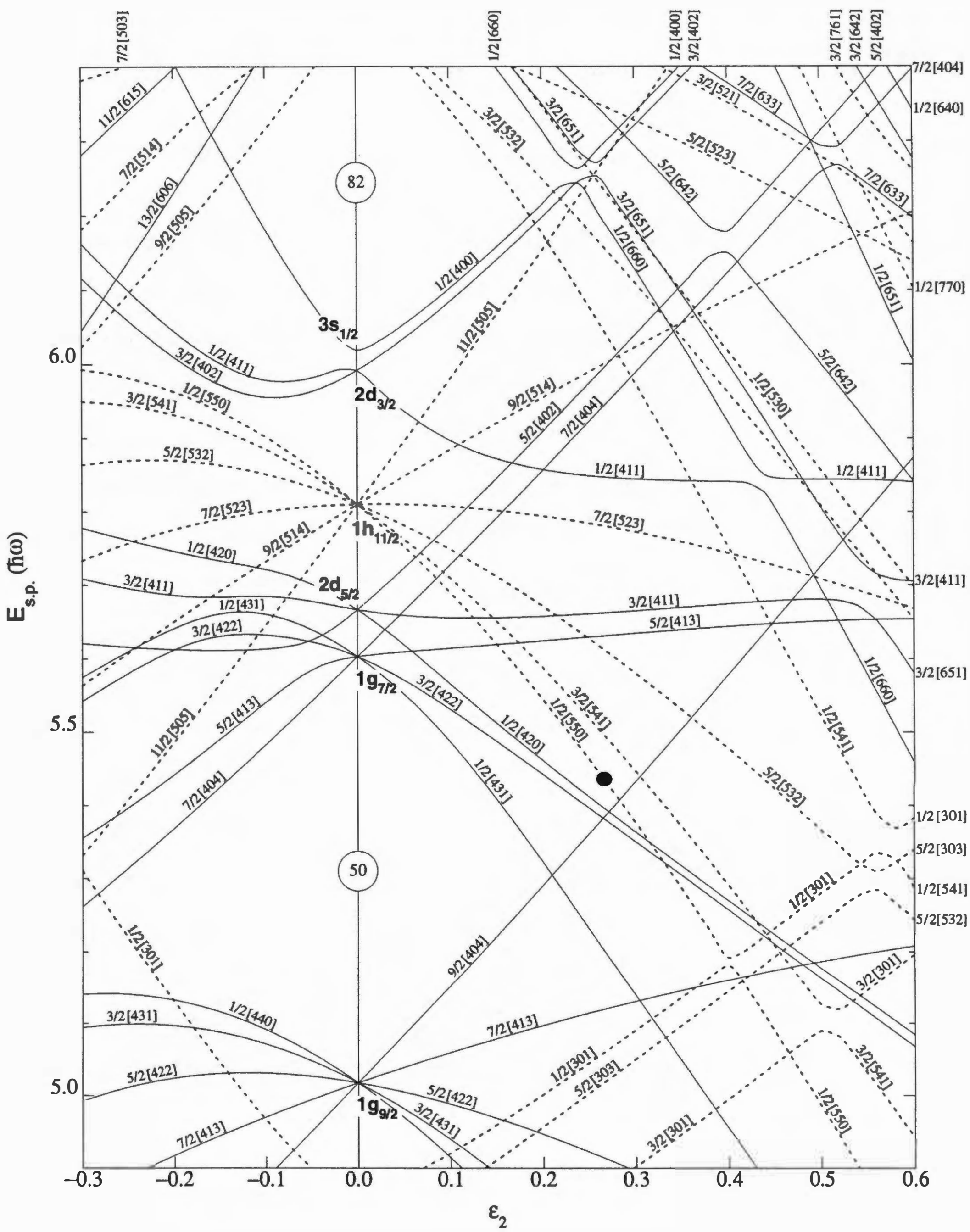

Figure 3.3: Nilsson diagram for protons, $50 \leq Z \leq 82$ ($\epsilon_4 = {\epsilon_2}^2/6$). The [550]1/2 proton orbital is identified near the Fermi surface.

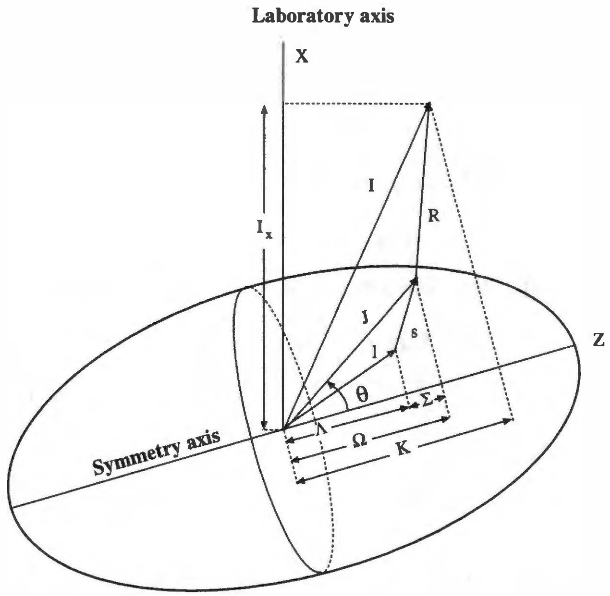

Figure 3.4: Diagram depicting a nucleon orbiting a deformed nucleus. The picture also defines the quantities J, K, and θ used with the Nilsson model. The symmetry axis is labeled as z.

of orbital angular momentum along the symmetry axis. An axially deformed nucleus has two axes of the same length and one of a different length. This latter axis is defined as the symmetry axis, z, as presented in Fig. 3.4. The projection of the j vector onto the symmetry axis is called as the Ω value of the orbital. With respect to a particular momentum j, the nucleon orbits the nucleus with a specific value of Ω which has a double degeneracy (either $|\Omega|$ or -$|\Omega|$) ranging from $|\Omega| = j, j-1, ..., 1/2$. Each Nilsson orbital has degeneracy of $(2j+1)$ nucleons. The parities[1] are indicated by solid lines for even ($\pi = +$) and dotted line for odd ($\pi = -$) in Fig. 3.3.

Understanding of this Nilsson diagram is essential to provide the orbital assignment for rotational bands in the nucleus of interest. From occupying the valence nucleons based on Pauli principle, the approximate position of the Fermi surface can be predicted at the ground-state deformation. In the case of ^{123}La, the proton $h_{11/2}[550]1/2$ orbital is identified to be near the Fermi surface with the predicted ground-state deformation $\beta = 0.27$ as shown in Fig. 3.3.

[1]The parity is given as $\pi = (-1)^l$ where l is the orbital angular momentum.

3.3 Description of Rotating Nuclei

3.3.1 Rotation

An important consequence of deformation is the rotational motion of the nucleus as a possible excitation mode. In the case of spherical nuclei, different orientations of the nucleus is not distinguishable. However, the rotation around the x or y axes can be measured for a deformed axially symmetric nucleus and the collective rotational energy is analogous to that of rotating rigid body in classical mechanics. The classical kinetic energy of this system is

$$E_{rot} = \frac{1}{2}\Im\omega^2 \tag{3.7}$$

where $\Im$ is the rotational moment of inertia and ω is a rotational frequency. By analogy to the quantum mechanical case, results in the following relation

$$E_l = \frac{\hbar^2}{2\Im^{(0)}}I(I+1). \tag{3.8}$$

In the equation above, $\Im^{(0)}$ is the static moment of inertia. Therefore, Eq. 3.8 suggests that the angular momentum states should be observed with an energy sequence of approximately $I(I+1)$ when a perfectly deformed nucleus is rotating. It is noted that the measured moment of inertia is less (30-50%) than the rigid rotor value at lower spin [18] because of the pairing interaction which makes the nucleus behave like a superfluid.

3.3.2 Cranked Shell Model

The simplest description of properties of rotating nuclei is the cranking-model approximation suggested by Inglis [19, 20]. Many successful studies of this model and its application can be found in the literature [21, 22, 23, 24, 25]. The cranking model provides a microscopic aspect of rotating nuclei where the total angular momentum is described as a sum of single-particle angular momenta, and therefore the collective and non-collective rotations can be treated on the same footing. The basic idea of the cranking model is that the nucleus having angular momentum $I \neq 0$ can be described by an intrinsic state ψ^ω at rest in a rotating frame. The Hamiltonian in the intrinsic rotating system

$$h^{\omega} = h - \hbar\omega j_x \tag{3.9}$$

is known as the cranking single-particle Hamiltonian where h is the single-particle Hamiltonian in an intrinsic rotating system and j_x is the x-component of the single-particle angular momentum. The term $-\omega j_x$ is analogous to the Coriolis and centrifugal forces in classical mechanics. These forces affect the intrinsic structure of a rotating nucleus. Depending on the direction of nuclear rotation, the Coriolis interaction breaks the time-reversal invariance and there is the preferential direction in nuclear rotation. The eigenvalues e_i^{ω} of the cranking Hamiltonian are referred to as the Routhian in the intrinsic rotating system. The summation over all the independent particles in the rotating system leads to the total cranking Hamiltonian in the laboratory system

$$H^{\omega} = H - \hbar\omega J_x \tag{3.10}$$

where ω is the angular frequency of the system, and J_x is the angular momentum operator along the rotational axis x perpendicular to the symmetry axis z. Through this process, experimental data can be compared with theoretical calculations. Although this model is very powerful for studying nuclear structure in the vicinity of yrast line, the cranking-model approximation has the limitation that the wave functions are not eigenstates of the angular momentum operator, since a rotation of the nucleus is externally imposed. Another disadvantage of the cranking model is that the approximation is poor for the crossing region where two rotational bands are interacting.

3.3.3 The Symmetries of the Hamiltonian

When the cranking Hamiltonian is used, the term $-\omega J_x$ breaks the time-reversal invariance because the rotation leads to a mixing of the single particle states. However, some symmetries are allowed to distinguish the single-particle states from different symmetry groups which do not mix. These symmetries are the parity (π) which describes space-reflection symmetry and signature (α) which represents the invariance with respect to a rotation of 180° about the rotation axis. The rotational operator is defined by

$$R_x(\pi)\psi_\alpha = e^{-i\pi j_1}\psi_\alpha = e^{-i\pi\alpha}\psi_\alpha, \tag{3.11}$$

where ψ_{alpha} is a wavefunction with signature α. The signature has values either $\alpha = +1/2$ or $\alpha = -1/2$. Although it is more common to use α for denoting the signature of rotational bands, signature may be indicated by the quantum number r, which is the eigenvalue of $R_x(\pi)$ and related to α, in the literature

$$r = e^{-i\pi\alpha}. \tag{3.12}$$

Therefore, the following relationship exists between α_{total} and the total angular momentum I for systems with an even number of nucleons

$$\begin{aligned} r &= +1 \;\; (\alpha = 0), \;\; I = 0, 2, 4, ... \\ r &= -1 \;\; (\alpha = 1), \;\; I = 1, 3, 5, ... \end{aligned} \tag{3.13}$$

while for systems with odd particle number

$$\begin{aligned} r &= -i \;\; (\alpha = +\frac{1}{2}), \;\; I = \frac{1}{2}, \frac{5}{2}, \frac{9}{2}, ... \\ r &= +i \;\; (\alpha = -\frac{1}{2}), \;\; I = \frac{3}{2}, \frac{7}{2}, \frac{11}{2}, ... \end{aligned} \tag{3.14}$$

Thus, the parity (π) and signature (α) are the only good quantum numbers to describe states in the CSM.

3.3.4 The Pairing Correlation

A critical feature of the interaction of nucleons in the nucleus is nucleon pairing. The Bardeen, Cooper, and Schrieffer (BCS) theory of superconductivity provided an important breakthrough in understanding pairing correlations in nuclei. The idea at the heart of superconductivity is that two electrons of opposite spin are paired into $I = 0$ states. This introduction gave rise to pairing gaps in nuclei for both protons and neutrons, just as for electron pairs in superconductors. The pairing causes every even-even nucleus to have a 0^+ ground state, which is well known from experimental evidence. Pairing also makes nuclei more bound when they have an even number of

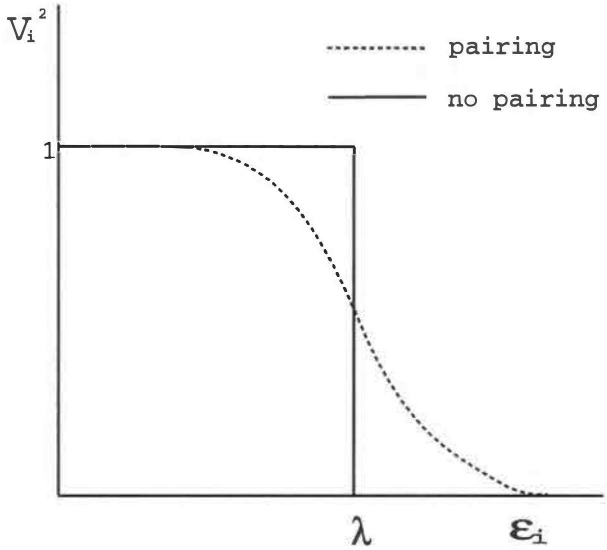

Figure 3.5: Representation of the Fermi Surface due to the pairing interaction.

protons and neutrons. The two particles travel in *time reversal orbits* when they orbit in the same j shell with projection Ω in opposite directions. The sum of the angular momenta in a pair is always equal to zero. A collision occurs between two particles and they scatter into another orbit. A pair orbiting in a particular j state has a chance to scatter back into the same or different j' state. Near the Fermi surface where there exists a probability that orbits are not occupied, this scattering can occur, which causes partial occupancy and changes the concept of particle and hole excitation. In the case of no pairing, orbits would be occupied sequentially based on the Pauli principle until all A nucleons had been placed in the lowest orbits. The effect of pairing on the the Fermi surface is displayed in Fig. 3.5. The partial occupancy near the Fermi surface leads to the concept of *quasiparticles* [18, 26]. Within the BCS treatment of pairing, the probability that a state i is occupied by a hole or a particle is given by

$$\begin{aligned} U_i^2 &= \frac{1}{2}\left[1 + \frac{\varepsilon_i - \lambda}{E_i}\right] \\ V_i^2 &= \frac{1}{2}\left[1 + \frac{\varepsilon_i - \lambda}{E_i}\right], \end{aligned} \tag{3.15}$$

where U_i^2 is the probability the orbit i is unoccupied and V_i^2 is the probability the orbit i is occupied. ε_i is the single-particle energy, and E_i is the energy necessary to excite a *quasiparticle* given by

$$E_i = \sqrt{(\varepsilon_i - \lambda)^2 + \Delta^2}, \tag{3.16}$$

with the pairing gap, Δ, and the Fermi surface denoted by λ. The normalization condition is $U^2 + V^2 = 1$. The pairing gap Δ and the number of particles n can be related to particle and hole occupation probabilities by

$$\Delta = G \sum_{i,j} U_i V_j \tag{3.17}$$

$$n = 2 \sum_i V_i^2. \tag{3.18}$$

It is evident that $V_i^2 = 1$ for $\varepsilon_i \ll \lambda$ and $U_i^2 = 1$ for $\varepsilon_i \gg \lambda$. The energy of 2Δ is required to excite a pair of nucleons to a higher state in even-even nuclei, while the valence nucleon is unpaired in odd-A nuclei.

3.4 Termination of Rotational Bands

A well-deformed nucleus normally increases its angular momentum by collective rotation. However, the collective angular momentum is built from contributions of the different nucleons outside closed shells (the valence nucleons) and is therefore limited. In a specific configuration, the contributions from the valence nucleons might reach their maximal values at some high-spin state. In such a *terminating state* [27, 28], all spin vectors are quantized along the rotation axis and the angular momentum is built as the sum of the *aligned spins* from individual nucleons (and nucleon holes) outside a closed shell. On its way to termination, a particular configuration will generally evolve continuously from high collectivity at low spin to a non-collective state at the highest spin. The nucleus migrates from prolate deformation ($\gamma = 0°$) through the (ε, γ)-plane to oblate ($\gamma = 60°$) shape during this transformation, which has been termed as (smooth) band termination. Such bands have been identified for example in $A \sim 110$ nuclei [27, 29, 30]. The corresponding configurations have one or two protons in $h_{11/2}$ orbitals and two proton holes in $g_{9/2}$ orbitals ($2p - 2h$ excitations across the $Z = 50$ shell gap). As the proton number increases above $Z = 53$, the terminating states involving proton holes will become experimentally inaccessible because they have very high spin and become unfavored energetically. Instead, terminating bands in configurations with a closed proton core might be observed. These configurations are analogous to those of the terminating bands in Dy/Er nuclei [31, 32, 33] in the sense that either the proton or the neutron configuration has a few particles outside a closed core ($Z = 50$ and $N = 82$) combined with a few neutrons or protons outside a "semi-closed" core of 64 neutrons or protons, and often with a few holes in this core. In order to investigate whether the observed phenomena are the results of a smooth band termination, cranked Nilsson-Strutinsky (CNS) calculations were performed similar to those in Ref. [27]. Since the most important features of terminating bands are revealed by their behavior in high spin, the neglect of pairing in CNS calculations has an advantage that tracing a particular configuration which experiences a dramatic deformation change is possible over the considerable spin range of band termination. The role of pairing correlations decreases due to blocking effects when the seniority of a configuration increases [34], as is the case for terminating bands. For a given configuration, pairing correlations are expected to decrease with increasing spin because of the Coriolis anti-pairing effect. These two effects mean that the correlated pairs outside a closed core are broken at very high rotational frequencies in terminating state. Therefore, pairing correlations are negligible. As pairing is not included in the calculations, they are realistic only above the spin values of approximately $25\hbar$ but they can give a general description about the most important configurations also at lower spin. The results of these calculations are shown together with experimental observables in chapter 5.

CHAPTER 4

Experimental Results in ^{123}La

4.1 Overview

The neutron-deficient nuclei in $A \sim 130$ are near mid-shell for neutrons ($N = 64$) and are thus very well deformed despite being only seven protons beyond the $Z = 50$ shell gap. Heavier La nuclei are noted as examples of shape coexistence at low spin due to competing shape driving effects from low-K protons (prolate driving) and high-K neutrons (oblate driving). At midshell, the neutrons are in the middle of the $h_{11/2}$ shell and are thus no longer strongly influencing the nuclear shape. It is in this spin region where smooth band termination [27] has been identified in ^{127,129}La [35, 36]. Characteristics of the lowest $(\pi, \alpha) = (+, -\frac{1}{2})$ band in ^{123}La are consistent with known properties of structures which are associated with exhibiting smooth band termination. Therefore, an investigation into possible termination in ^{123}La has been performed by comparing experimental data with cranked Nilsson-Strutinsky calculations.

4.2 Experimental Details

The reaction ^{40}Ca + ^{92}Mo was used to produce these light rare-earth nuclei with $Z = 57 - 60$. A beam energy of 184 MeV was selected and the target consisted of a 0.625 mg/cm^2 self-supporting foil of ^{92}Mo. The experiment was performed at Argonne National Laboratory and utilized Gammasphere [37] in combination with the Washington University Microball [38]. Gammasphere consisted of 99 Ge detectors for this experiment. Although ^{123}La was populated in a relatively weak reaction channel (~1.3% of the ~580 million five-fold or higher events recorded), the selectivity of the

Microball allowed for an extremely clean separation of γ rays in coincidence with the $2\alpha p$ channel leading to ^{123}La. These transitions were corrected for Doppler shifts and sorted into an $E_\gamma \times E_\gamma \times E_\gamma$ cube that was inspected with the Radware [12] package.

The relative spin assignments were determined through a directional angular correlation of oriented states (DCO) analysis. To obtain this information with sufficient statistics, an angular-dependent $E_\gamma \times E_\gamma$ matrix was created where the energies of γ rays observed in detectors located at 31.7°, 37.4°, 50.1°, 129.9°, 142.6°, and 148.3° (symmetric forward and backward, FB, angles) were projected along one axis and coincident γ rays observed in detectors located at 79.2°, 80.7°, 90.0°, 99.3°, and 100.8° were projected along the other. DCO ratios were determined by the following expression

$$R_{DCO} = \frac{I_{\gamma_1}(\text{at FB, in coincidence with } \gamma_2 \text{ at } \sim 90^\circ)}{I_{\gamma_1}(\text{at } \sim 90^\circ, \text{ in coincidence with } \gamma_2 \text{ at FB})}$$

where I_{γ_1} is the intensity of the γ ray of interest and γ_2 is a stretched $E2$ ($\Delta I = 2$) transition. With the detectors at the given angles, expected R_{DCO} values are approximately 0.5 for pure dipole transitions ($M1$ and $E1$) and 1.0 for quadrupole transitions ($E2$). The measured DCO ratios are summarized in Table 4.1 along with the energy, spin, and parity of the states, as well as the relative intensity of the depopulating γ rays. Where the statistics were too low to perform DCO analysis, multipolarities were assigned assuming that rotational band characteristics persist.

4.3 The Level Scheme

In an earlier work on ^{123}La [7], three rotational bands were identified without any linking transitions observed between the bands. The level scheme for ^{123}La deduced from the present work is shown in Fig. 4.1.

The previously known structures are labeled as bands 1, 3, and 6 in Fig. 4.1 and were extended to much higher spin. Three new structures, labeled as bands 2, 4, and 5, were also identified. Linking transitions were established for the first time between bands 1-5 such that relative excitation energies of these sequences are now

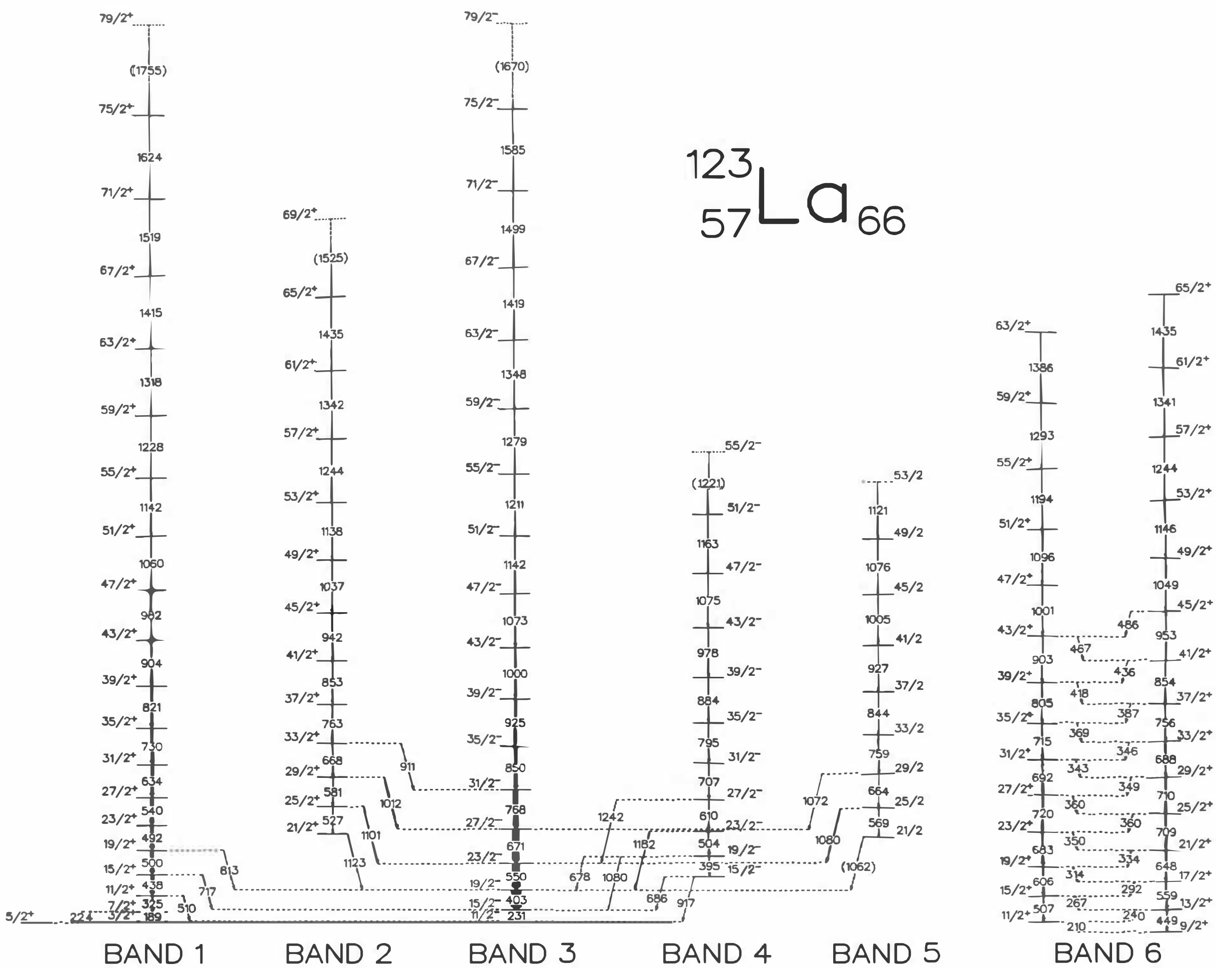

Figure 4.1: The level scheme for ^{123}La. The width of the arrows is proportional to the intensity of the transition. Tentative transitions are denoted by dashed lines. Spin and parity assignments are considered tentative as explained in the text.

Table 4.1: Gamma-ray energies and intensities in ^{123}La.

$I_i^{\pi [1]}$	E_{level} (keV)	E_γ (keV)[2]	I_γ[3]	DCO
		BAND 1		
$\frac{7}{2}^+$	224.4	189.0	12.9(6)	0.91(2)
		224.4	~5	0.69(4)
$\frac{11}{2}^+$	549.2	324.9	23(1)	0.93(2)
		509.9	4.4(3)	0.51(5)
$\frac{15}{2}^+$	987.4	438.2	35(1)	0.98(2)
		717.0	3.9(2)	0.61(11)
$\frac{19}{2}^+$	1487.4	500.0	37(2)	1.02(2)
		812.7	<2	
$\frac{23}{2}^+$	1979.4	492.0	36(1)	0.96(2)
$\frac{27}{2}^+$	2519.0	539.6	32(1)	1.08(2)
$\frac{31}{2}^+$	3152.6	633.6	30.7(9)	1.11(3)
$\frac{35}{2}^+$	3882.7	730.1	27.0(7)	0.95(2)
$\frac{39}{2}^+$	4703.5	820.8	21.6(5)	1.05(5)
$\frac{43}{2}^+$	5607.5	904.0	15.9(4)	1.09(4)
$\frac{47}{2}^+$	6589.7	982.2	11.3(3)	1.17(5)
$\frac{51}{2}^+$	7650.1	1060.4	7.7(2)	1.10(7)
$\frac{55}{2}^+$	8791.8	1141.7	5.4(8)	1.02(8)
$\frac{59}{2}^+$	10020.1	1228.3	2.9(2)	1.02(12)
$\frac{63}{2}^+$	11338.2	1318.1	<2	
$\frac{67}{2}^+$	12753.0	1414.8	<2	
$\frac{71}{2}^+$	14272.2	1519.2	<2	
$\frac{75}{2}^+$	15896.4	1624.2	<2	
$\frac{79}{2}^+$	(17650.9)	(1755)	<2	

Table 4.1 (continued).

I_i^{π}[1]	E_{level} (keV)	E_γ (keV)[2]	I_γ[3]	DCO
		BAND 2		
$\frac{21}{2}^+$	1565.5	1122.9	3.9(4)	
$\frac{25}{2}^+$	2092.9	527.4	6.5(3)	
		1101.2	9.1(5)	0.46(7)
$\frac{29}{2}^+$	2673.5	580.6	7.1(4)	
		1011.5	12.1(6)	0.56(4)
$\frac{33}{2}^+$	3341.6	668.1	10.0(5)	
		911.3	7.5(3)	0.64(4)
$\frac{37}{2}^+$	4104.2	762.6	10.4(6)	
$\frac{41}{2}^+$	4957.1	852.9	10.2(5)	
$\frac{45}{2}^+$	5898.9	941.8	9.7(5)	
$\frac{49}{2}^+$	6935.8	1036.9	8.8(4)	
$\frac{53}{2}^+$	8074.1	1138.3	4.1(2)	
$\frac{57}{2}^+$	9317.9	1243.8	3.5(2)	
$\frac{61}{2}^+$	10660.1	1342.2	<2	
$\frac{65}{2}^+$	12094.7	1434.6	<2	
$\frac{69}{2}^+$	(13619.6)	(1524.9)	<2	
		BAND 3		
$\frac{15}{2}^+$	39.3	230.7	~120	0.91(1)
$\frac{19}{2}^+$	442.6	403.3	≡100	0.94(2)
$\frac{23}{2}^+$	992.6	550.0	83(4)	1.00(1)
$\frac{27}{2}^+$	1663.2	670.6	71(3)	1.00(2)
$\frac{31}{2}^+$	2431.2	768.0	50(2)	1.02(3)

Table 4.1 (continued).

I_i^{π}[1]	E_{level} (keV)	E_γ (keV)[2]	I_γ[3]	DCO
$\frac{35}{2}^+$	3280.9	849.7	31(2)	1.00(4)
$\frac{39}{2}^+$	4206.3	925.4	24(1)	0.97(4)
$\frac{43}{2}^+$	5206.7	1000.4	16.3(6)	1.00(5)
$\frac{47}{2}^+$	6279.7	1073.0	13.3(6)	0.94(7)
$\frac{51}{2}^+$	7421.6	1141.9	9.6(4)	1.37(9)
$\frac{55}{2}^+$	8632.3	1210.7	4.8(2)	
$\frac{59}{2}^+$	9911.1	1278.8	4.5(2)	
$\frac{63}{2}^+$	11259.1	1348.0	<2	
$\frac{67}{2}^+$	12678.5	1419.4	<2	
$\frac{71}{2}^+$	14177.2	1498.7	<2	
$\frac{75}{2}^+$	15761.9	1584.7	<2	
$\frac{79}{2}^+$	(17432.0)	(1670.1)	<2	
		BAND 4		
$\frac{15}{2}^+$		686.0	2.0(0)	
	956.3	917.0	<2	
$\frac{19}{2}^+$	1351.0	394.7	3.4(1)	
		678.0	2.5(0)	
$\frac{23}{2}^+$		1080.1	<2	
	1855.3	504.3	6.0(3)	
$\frac{27}{2}^+$		1182.3	6.1(4)	
	2465.6	610.3	6.7(4)	
$\frac{31}{2}^+$		1242.1	<2	
$\frac{35}{2}^+$	3172.4	706.8	5.2(3)	
$\frac{39}{2}^+$	3967.4	795.0	8.2(5)	

Table 4.1 (continued).

I_i^{π} [1]	E_{level} (keV)	E_γ (keV)[2]	I_γ [3]	DCO
$\frac{39}{2}^+$	4851.1	883.7	6.1(3)	
$\frac{43}{2}^+$	5829.3	978.2	5.5(3)	
$\frac{47}{2}^+$	6904.6	1075.3	3.4(3)	
$\frac{51}{2}^+$	8067.3	1162.7	2.1(0)	
$\frac{55}{2}^+$	9288.3	1221.0	2.4(0)	
		BAND 5		
$\frac{23}{2}^+$	(1735.5)	(1062.2)	5.9(4)	
$\frac{27}{2}^+$	2304.3	568.8	2.9(0)	
		1080.0	5.5(4)	
$\frac{31}{2}^+$	2968.6	664.3	<2	
		1072.0	<2	
$\frac{35}{2}^+$	3727.6	759.0	7.1(4)	
$\frac{39}{2}^+$	4571.5	843.9	4.3(3)	
$\frac{43}{2}^+$	5498.5	927.0	2.9(0)	
$\frac{47}{2}^+$	6503.8	1005.3	4.4(3)	
$\frac{51}{2}^+$	7579.9	1076.1	<2	
$\frac{55}{2}^+$	8701.1	1121.2	<2	
		BAND 6		
$\frac{11}{2}^+$	X+209.5	209.5	~30	0.55(6)
$\frac{15}{2}^+$	X+716.1	506.6	10.2(5)	
		267.1	23(1)	0.55(6)

Table 4.1 (continued).

I_i^{π}[1]	E_{level} (keV)	E_γ (keV)[2]	I_γ[3]	DCO
$\frac{19}{2}^+$	X+1322.4	606.3	13.1(6)	
g		314.4	15.4(6)	0.52(5)
$\frac{23}{2}^+$	X+2005.0	682.6	13.0(6)	
		349.7	7.4(3)	0.58(6)
$\frac{27}{2}^+$	X+2724.7	719.7	11.9(6)	
		359.5	7.0(3)	0.58(6)
$\frac{31}{2}^+$	X+3417.0	692.3	11.3(6)	
		342.9	4.5(2)	0.55(6)
$\frac{35}{2}^+$	X+4132.1	715.1	7.8(4)	
		369.2	4.0(2)	0.54(7)
$\frac{39}{2}^+$	X+4937.4	805.3	7.8(4)	
		417.9	2.2(2)	0.53(8)
$\frac{43}{2}^+$	X+5840.8	903.4	5.3(3)	
		467.0	1.8(1)	
$\frac{47}{2}^+$	X+6842.1	1001.3	5.0(3)	
$\frac{51}{2}^+$	X+7938.0	1095.9	4.8(3)	
$\frac{55}{2}^+$	X+9132.3	1194.3	2.9(2)	
$\frac{59}{2}^+$	X+10425.2	1292.9	<2	
$\frac{63}{2}^+$	X+11810.9	1385.7	<2	
		BAND 6		
$\frac{13}{2}^+$	X+449.2	449.2	6.0(3)	
		239.5	31(1)	0.58(6)
$\frac{17}{2}^+$	X+1008.5	559.3	13.4(6)	
		292.1	18.5(8)	0.54(6)

Table 4.1 (continued).

I_i^{π}[1]	E_{level} (keV)	E_γ (keV)[2]	I_γ[3]	DCO
$\frac{21}{2}^+$	X+1656.3	647.8	13.4(6)	
		333.6	11.5(5)	0.59(6)
$\frac{25}{2}^+$	X+2365.5	709.2	13.4(7)	
		360.1	7.2(4)	0.57(6)
$\frac{29}{2}^+$	X+3075.1	709.6	12.9(7)	
		349.4	7.4(4)	0.58(6)
$\frac{33}{2}^+$	X+3763.3	688.1	9.8(5)	
		346.1	3.7(2)	
$\frac{37}{2}^+$	X+4519.5	756.3	9.4(4)	
		387.1	2.9(2)	0.72(17)
$\frac{41}{2}^+$	X+5373.8	854.3	7.2(4)	
		436.4	1.8(2)	0.55(7)
$\frac{45}{2}^+$	X+6326.8	953.0	5.1(3)	
		485.8	1.7(1)	
$\frac{49}{2}^+$	X+7375.8	1049.0	5.1(3)	
$\frac{53}{2}^+$	X+8521.9	1146.1	5.1(3)	
$\frac{57}{2}^+$	X+9765.6	1243.7	4.0(2)	
$\frac{61}{2}^+$	X+11107.0	1341.4	<2	
$\frac{65}{2}^+$	X+12541.9	1434.9	<2	

[1] Spin and parity of the depopulated state.

[2] Uncertainties in E_γ are 0.2 keV for most transitions except for relatively weak transitions which are 0.5 keV.

[3] Relative intensity of the transition where $I_\gamma(403.3) \equiv 100$.

known. The ordering of transitions in the level scheme was based on the observed coincidence relationships and measured relative intensities. Spin and parity assignments for bands 1, 3, and 6 were suggested by Wyss *et al.* [7] on the basis of systematics, observed band crossing behavior, and the single-particle orbitals expected near the Fermi surface. We are in agreement with these assignments, however, these, along with all new assignments, must be considered as tentative since the spin/parity of the ground state has not been firmly established.

Prior to our work, band 1 was reported up to $I^\pi = \frac{55}{2}^+$ [7], and is now extended to $I^\pi = (\frac{79}{2}^+)$. A spectrum of band 1 is given in Fig. 4.2(a), which is a result of summing all possible combinations of double gates above the $\frac{35}{2}$ state. There are two transitions decaying from the $\frac{7}{2}$ state with energies of 189.0 keV and 224.4 keV (see Fig. 4.1). A DCO ratio of 0.91(2) suggests that the former γ ray is an $E2$ transition while the 224.4-keV γ ray is likely a ΔI=1 transition due to its measured R_{DCO}=0.69(4). Thus, the 189.0-keV transition is placed as an inband transition in Fig. 4.1 and the 224.4-keV γ ray is shown as a decay to the lowest observed state in ^{123}La. It is possible that this is the ground state, however, a recent β decay experiment could not determine the ground-state spin or parity [39].

Although band 1 is $\sim$ 700 keV above the yrast sequence (band 3) at low spin ($I \leq \frac{15}{2}$), it becomes yrast at and above $I = \frac{51}{2}$. Linking transitions were observed between bands 1 and 3 (see Fig. 4.1) and a DCO ratio of 0.6(1) was determined for the 717-keV transition. Given the proposed spins for band 3 (see below), the 987.4-keV state was assigned $I = \frac{15}{2}$ resulting in a bandhead spin of $\frac{3}{2}$. This is in good agreement with the proposed configuration of band 1, as discussed below, and the assignment in Ref. [7].

As previously stated, band 2 was observed for the first time and a representative spectrum is shown in Fig. 4.2(b). The four lowest states of this band strongly feed band 3 through high-energy transitions. The DCO analysis indicates that the 911.3-keV, 1011.5-keV, and 1101.2-keV linking transitions are nearly pure dipoles which is suggestive that they are likely $E1$ transitions. Thus, $I^\pi = \frac{21}{2}^+$ has been assigned to the 1565.5-keV level in band 2 as odd parity is associated with band 3 (see below). It is interesting to note that while bands 1 and 2 both have even parity,

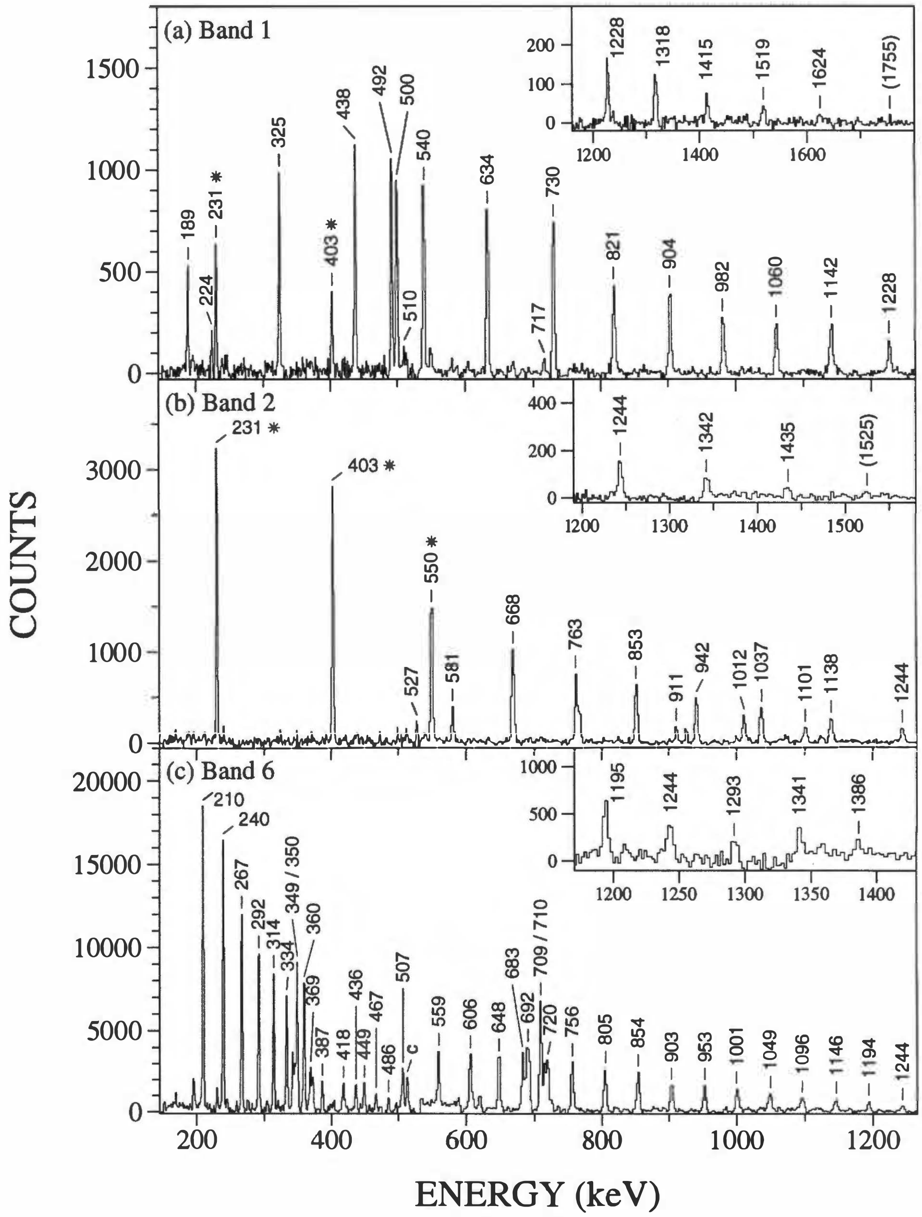

Figure 4.2: Spectra of bands 1, 2, and 6. (a) Spectrum of band 1 is produced by summing all possible combinations of double gates above the $\frac{35}{2}$ state. (b) Spectrum for band 2 is a result of many double-gated γ ray coincidence spectra. (c) For strongly coupled band 6, the spectrum is obtained in a similar manner as stated above. The high energy transitions of all bands are displayed in insets, and peaks denoted by $*$ are associated with band 3.

no linking transitions between the sequences were observed. Band 2 was observed up to a relatively high angular momentum state of ($\frac{73}{2}$).

Band 3, as displayed in the level scheme of Fig. 4.1, is the most intensely populated structure at lower spins in ^{123}La. Wyss *et al.* [7] proposed the $\frac{11}{2}^-$ assignment for the initial state based on the systematics of heavier La isotopes and its suggested configuration. In a β-decay study [39], states of spin $\frac{7}{2}$, $\frac{9}{2}$, and $\frac{11}{2}$ in ^{123}Ba were directly fed by ^{123}La. This indicates the presence of a high-spin ground state or β-decaying isomer in ^{123}La. From the present work, it is clear that the $\frac{11}{2}^-$ level is not the ground state as it lies 4 keV above the bandhead of band 1 and 39.4 keV above the lowest state observed. However, as the γ transition decaying from the $\frac{11}{2}^-$ bandhead of band 3 to the possible ground state is low energy ($\sim$ 39 keV) and large multipolarity (perhaps $E3$), the lifetime of the $\frac{11}{2}^-$ state is likely large and may indicate β decay. The present data allowed for the extension of this band from $\frac{59}{2}^-$ to $\frac{79}{2}^-$ and a spectrum is given in Fig. 4.3(a).

The lowest state in band 4 was observed at an energy of 956.3 keV and it decays into both the $\frac{11}{2}$ and $\frac{15}{2}$ states of band 3. These linking transitions, plus those coming from higher spin states, can be observed in the sample spectrum provided in Fig. 4.3(b). This decay pattern limits the choices of spin for the lowest state to either $\frac{13}{2}$ or $\frac{15}{2}$ as only $E1$, $M1$, and $E2$ transitions are normally observed in prompt spectroscopy. Unfortunately, the linking transitions from this structure to band 3 were too weak to obtain meaningful DCO ratios. A spin of $\frac{15}{2}$ is favored for the 956.3 keV state based upon energy and population intensity considerations; however, the $\frac{13}{2}$ assignment cannot be completely excluded. In addition, the decay and inband characteristics of this sequence are similar to a structure in ^{125}La (labeled as band 6 in Ref. [40]) whose lowest state was determined to be $\frac{15}{2}^-$. The assignment of $\frac{15}{2}$ to the lowest state in band 4 requires negative parity for this band, in view of the transition to the $\frac{11}{2}^-$ state.

The weakest observed structure in ^{123}La is denoted as band 5 in Fig. 4.1 and a spectrum is presented in Fig. 4.3(c). Once again, relative spin assignments could not be assigned by DCO analysis due to insufficient statistics. However, since band 5 was seen as high in energy as band 4, it is likely that these bands are relatively

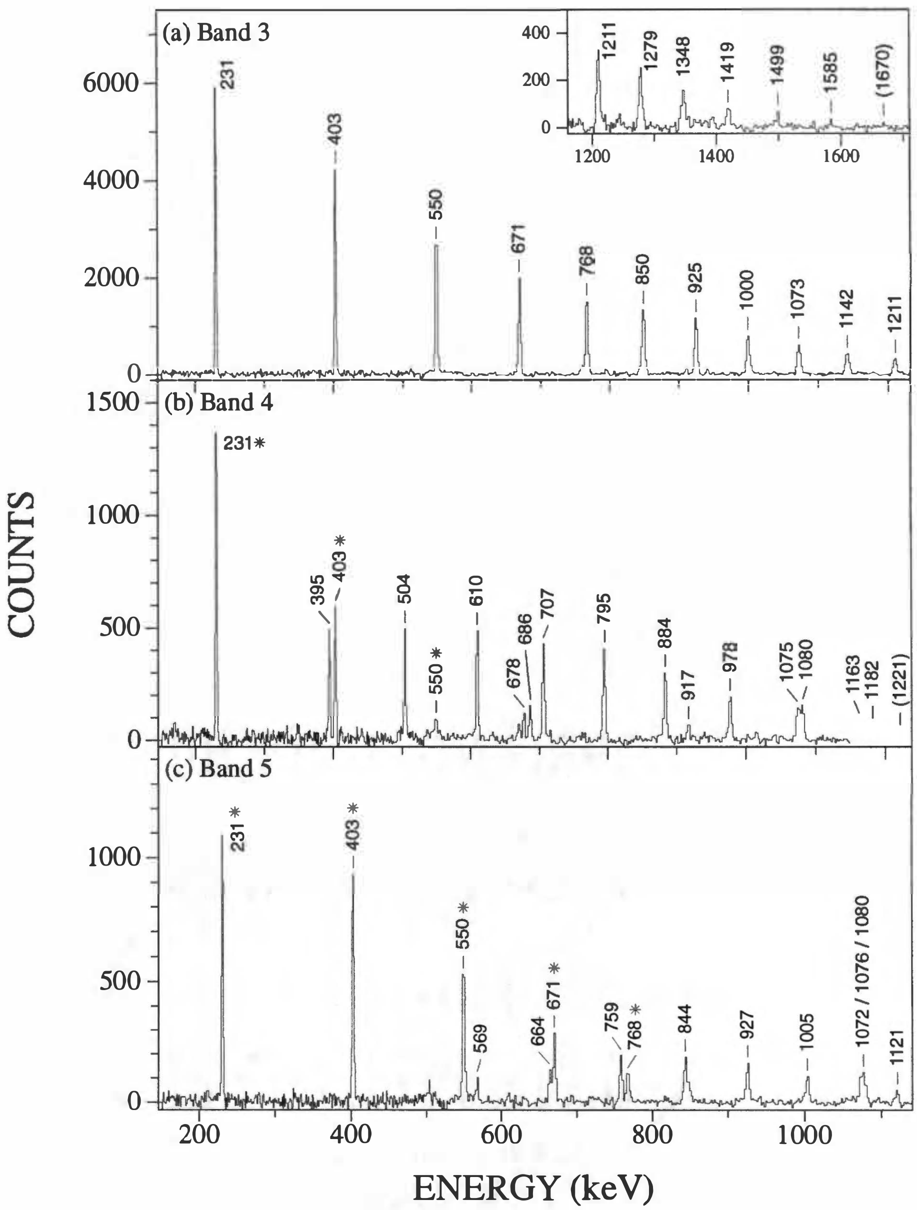

Figure 4.3: Spectra of bands 3, 4, and 5. (a) A sum of many double-gated transitions provides the representative spectrum of ground-state band in ^{123}La. Spectra in panel (b) and (c) for bands 4 and 5 are produced from summing individual gated spectra and show the coincidence relationship denoted by $*$ with band 3.

close in energy at their highest observed spins. Therefore, a spin of $I = \frac{21}{2}$ has been tentatively assigned for the lowest state, which suggests that the linking transitions to band 3 are likely dipoles. No parity assignment has been made as a definitive configuration for this sequence.

The strongly-coupled sequence labeled as band 6 in Fig. 4.1, was assigned a $\frac{9}{2}^+$ bandhead spin/parity based on the proposed configuration in Ref. [7]. This structure was extended to $\frac{65}{2}^+$ with the present data and a spectrum for both signatures is shown in Fig. 4.3(c). No linking transitions were observed between this structure and the other bands in ^{123}La. Indeed, inspection of Fig. 4.3(c) reveals that there are no coincidence relations with any of the other sequences. Thus, it is likely that band 6 also has an isomeric bandhead state with a lifetime greater than that of the prompt time gate (~80 ns) used for this analysis. It should be noted that a similar structure in ^{125}La [40] appears to be based on an isomeric state as well.

4.4 Configuration Assignments

In order to facilitate a discussion of the configurations for the structures in ^{123}La, the aligned angular momenta of bands 1-6 are plotted as a function of rotational frequency in Fig. 4.4. The ground-state band of ^{122}Ba [41, 42], which is the core nucleus of ^{123}La, is also plotted for comparison. Harris parameters [43] $\mathcal{J}_0 = 17.0$ $\hbar^2$/MeV and $\mathcal{J}_1 = 25.8$ $\hbar^4$/MeV^3 were adopted from previous studies [7] to subtract the angular momentum of the collective core. Observed band crossings are labeled using an alphabetic labeling scheme [44] (see Table 4.2) in which the most favored $h_{11/2}$ protons and neutrons (with signatures $\alpha = -\frac{1}{2}$ and $+\frac{1}{2}$) are denoted as E_p, F_p and E, F, respectively. The second favored pair of $h_{11/2}$ protons are known as G_p and H_p.

Cranked shell model (CSM) [45] calculations were performed using deformation parameters (β_2, β_4, and γ) determined by total Routhian surface (TRS) [46] calculations in order to interpret the observed crossings and are presented in Fig. 4.5. With a predicted ground-state deformation of $\beta_2 = 0.27$ for ^{123}La, the bands based on the $h_{11/2}[550]1/2$, $d_{5/2}[420]1/2$, $g_{7/2}[422]3/2$, and $g_{9/2}[404]9/2$ orbitals were previously

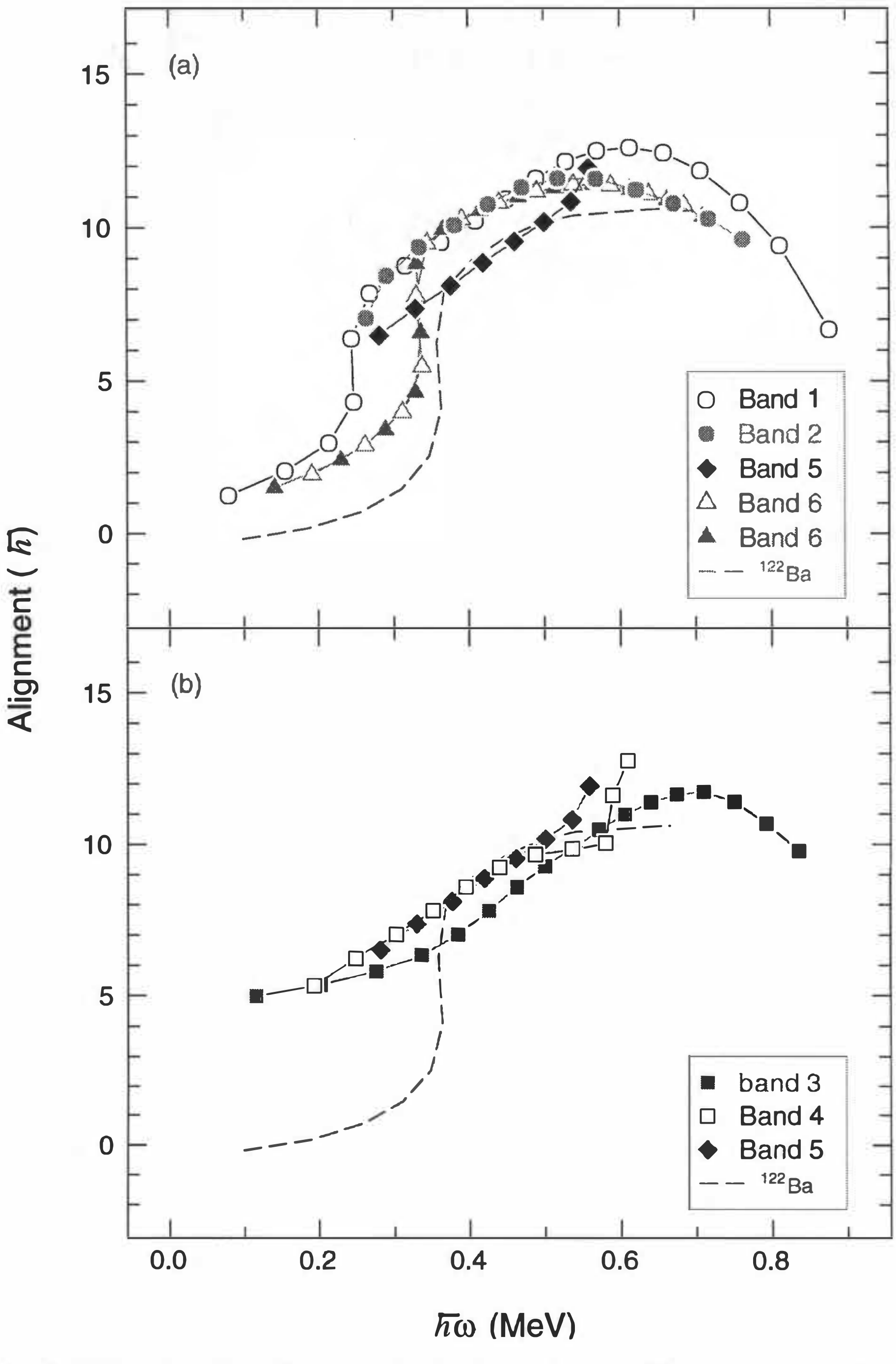

Figure 4.4: Aligned angular momentum versus rotational frequency for (a) bands 1, 2, 5, and 6, as well as (b) bands 3, 4, and 5 in ^{123}La. The ground-state band in ^{122}Ba is included for comparison purposes. Harris parameters $\mathcal{J}_0 = 17.0\ \hbar^2/\text{MeV}$ and $\mathcal{J}_1 = 25.8\ \hbar^4/\text{MeV}^3$ were used to subtract the angular momentum of the core.

Table 4.2: Alphabetic quasiparticle labeling scheme for ^{123}La.

Label	$(\pi, \alpha)_n$ [1]	Configuration [2]	Label	$(\pi, \alpha)_n$ [1]	Configuration [2]
		Quasiprotons			
A_p	$(+,+\frac{1}{2})_1$	[422]3/2	B_p	$(+,-\frac{1}{2})_1$	[422]3/2
C_p	$(+,+\frac{1}{2})_2$	[420]1/2	D_p	$(+,-\frac{1}{2})_2$	[420]1/2
X_p	$(+,+\frac{1}{2})_3$	[404]9/2	Y_p	$(+,-\frac{1}{2})_3$	[404]9/2
E_p	$(-,-\frac{1}{2})_1$	[550]1/2	F_p	$(-,+\frac{1}{2})_1$	[550]1/2
		Quasineutrons			
E	$(-,-\frac{1}{2})_1$	$h_{11/2}$	F	$(-,+\frac{1}{2})_1$	$h_{11/2}$

[1] Parity (π) and signature (α) of the orbital. The subscript n numbers the quasiparticle excitations of a specific signature and parity starting with the lowest in energy at $\hbar\omega = 0$ MeV.

[2] Configuration of the orbital at $\hbar\omega = 0$ MeV.

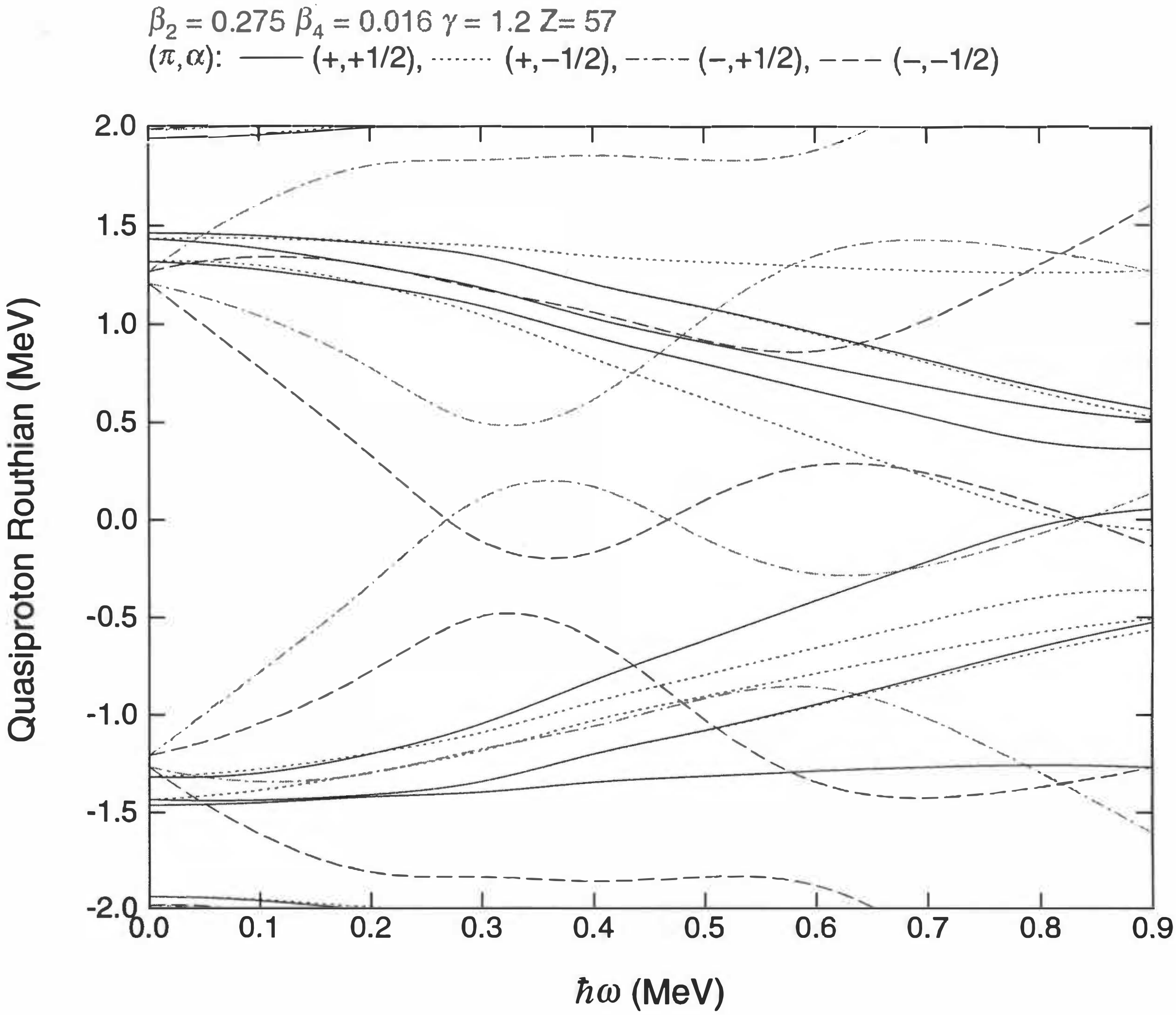

Figure 4.5: Quasiproton Routhians calculated within the Cranked Shell Model for ^{123}La. Deformations are listed in the figure and were derived from total Routhian surface calculations.

suggested to be near the Fermi surface at $Z = 57$ [7]. Band characteristics such as alignment behavior and $B(M1)/B(E2)$ ratios are discussed to associate the observed bands in ^{123}La with the orbitals mentioned above.

4.4.1 Band 1

A large alignment gain is observed at a crossing frequency of $\hbar\omega_c \approx 0.26$ MeV for band 1. As seen in Fig. 4.4(a), the ground-state band in ^{122}Ba displays a similar gain in alignment, but the crossing occurs at a higher frequency of $\hbar\omega_c \approx 0.36$ MeV. Both crossings are interpreted as resulting from the alignment of the lowest $h_{11/2}$ quasiprotons (E_pF_p) which are the only orbitals near the Fermi surface that can produce this large increase in angular momentum. Since the E_pF_p crossing is observed in band 1, the [550]1/2 configuration is excluded as this crossing would be Pauli blocked. A strongly-coupled sequence is expected with the [404]9/2 configuration; thus, band 1 is likely a mixture of the low-K $d_{5/2}$ and $g_{7/2}$ orbitals. Although band 1 is a mixture of these two even-parity states, one can determine which orbital likely dominates the wave function from the observed favored signature. The favored signature is normally dependent upon the j of the shell as $\alpha_f = (-1)^{j-1/2}$; thus, $\alpha_f = +\frac{1}{2}$ for $d_{5/2}$ and $\alpha_f = -\frac{1}{2}$ for $g_{7/2}$. As band 1 has $\alpha = -\frac{1}{2}$ and is the most favored even-parity sequence, it is likely best associated with the $g_{7/2}$[422]3/2 orbital (see Fig. 3.3). This is in good agreement with the proposed bandhead spin assignment.

One may note that the CSM calculations predict the E_pF_p crossing to occur near 0.35 MeV (see Fig. 4.5). Although this prediction appears to be in good agreement with the crossing frequency of the ground-state sequence in ^{122}Ba, the theoretical value is higher than the experimental crossing frequency observed in band 1. A similar phenomenon was reported for the lowest $(\pi, \alpha) = (+, -\frac{1}{2})$ configuration in ^{125,127,129}La [40, 47, 36] and ^{121}Cs [48]. Wyss *et al.* [7] investigated the possibility that the influence of quadrupole pairing could be the cause for the difference in crossing frequencies between this sequence and the ground-state band in ^{122}Ba. By including a quadrupole pairing term in the Hamiltonian, it was found that blocking a down-sloping orbital reduces the pairing field. Indeed, their calculations reproduced the

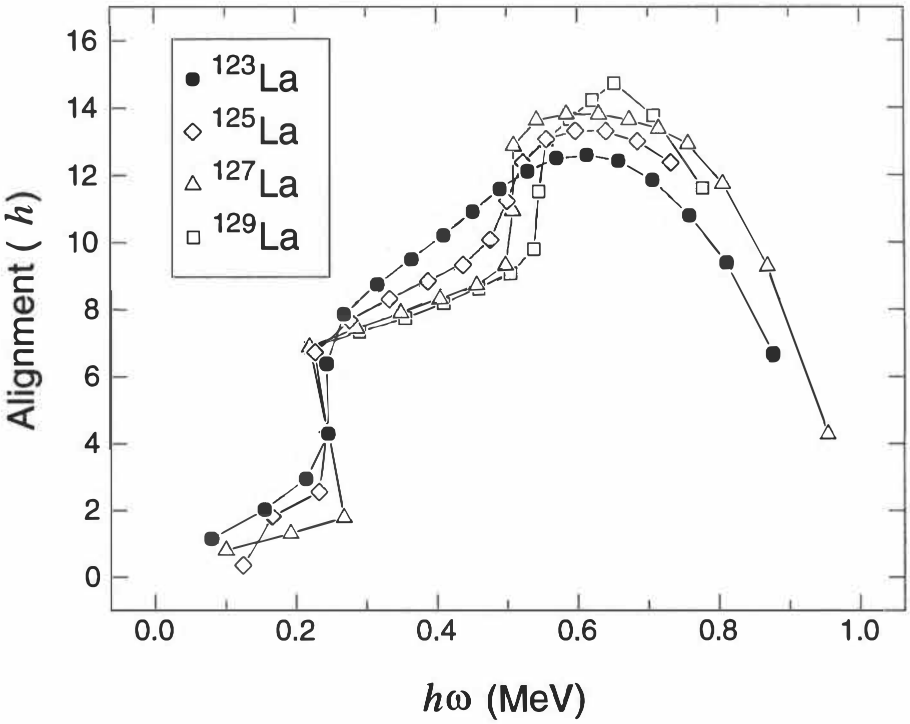

Figure 4.6: Alignment of $\pi d_{5/2}/g_{7/2}[422]3/2$ bands in ^{123,125,127,129}La. Harris parameters of $\mathcal{J}_0 = 17.0\ \hbar^2/\text{MeV}$ and $\mathcal{J}_1 = 25.8\hbar^4\ /\text{MeV}^3$ were used for each nucleus.

crossing frequency for band 1 by reducing the proton pairing gap, Δ_p, by 25% compared to that of the ground-state band in ^{122}Ba. Such effects are amplified in regions where the level density is low, in this case where the proton Fermi surface is near the $Z = 50$ shell gap. However, blocking an up-sloping orbital, such as $g_{9/2}[404]9/2$, does not influence the pairing strength nearly as much [49], and a "normal" crossing frequency can be expected in such bands.

A gradual gain in alignment is observed in band 1 following the E_pF_p crossing. In order to identify the nature of this rise, the alignments of the [422]3/2 bands in ^{123,125,127,129}La have been plotted in Fig. 4.6. One may observe that a second crossing, which has been attributed to the rotational alignment of $h_{11/2}$ neutrons (EF crossing), is quite noticeable in the three heavier La nuclei. A trend in the crossing frequency can be established from this plot where the alignment occurs at successively lower frequencies with decreasing neutron number. This is the result of lowering the neutron Fermi surface in the $h_{11/2}$ shell such that lower Ω orbitals are occupied. It takes less energy to align these orbitals, thus this is an expected trend. Another feature that can be discerned from Fig. 4.6 is that the interaction strength increases significantly for the EF crossing between ^{125}La and ^{127}La. A systematic study of the EF crossing in Cs nuclei revealed increasing interaction strength as N decreases from 74 to 66 [48]. In fact, ^{121}Cs, the isotone of ^{123}La, displays the largest interaction strength. It was suggested that an increase in neutron-proton interactions causes the stronger band mixing [48]. Thus, one may expect a large interaction strength for this crossing in ^{123}La as well, and the alignment gain near 0.44 MeV in band 1 is interpreted as the EF crossing. This frequency is in good agreement with the CSM prediction of $\hbar\omega_c \approx 0.42$ MeV (not shown). The alignment appears to decrease following the EF crossing; however, this is likely the result of improper Harris parameters for the high-frequency, five-quasiparticle region.

4.4.2 Band 2

The lowest observed state in band 2 is at 1796.3 keV indicating that it is initially a three-quasiparticle structure. Inspection of the alignments for bands 1 and 2, shown in Fig. 4.4(a), reveals that the two have nearly overlapping values between $\hbar\omega = 0.25$-0.45 MeV. This indicates band 2 is observed following the E_pF_p crossing that likely occurs at a low crossing frequency similar to band 1. Thus, it is most plausible that bands 1 and 2 have similar configurations, and the latter is assigned the $\pi(d_{5/2}/g_{7/2})E_pF_p$ configuration. Since band 2 has the opposite signature of band 1, it is a mixture of the signature partner of band 1 and the favored signature ($\alpha = +1/2$) of the $\pi d_{5/2}$ sequence. The lack of linking transitions between these two sequences suggests that the latter component may be more favored. Once again, the gradual gain in alignment near $\hbar\omega = 0.4$ MeV is attributed to the EF crossing and no further crossings are observed in band 2 up to $\hbar\omega \approx 0.7$ MeV.

4.4.3 Band 3

Figure 4.4(b) displays the aligned angular momentum for band 3. This structure does not experience the low frequency crossing observed in band 1 or in the ground-

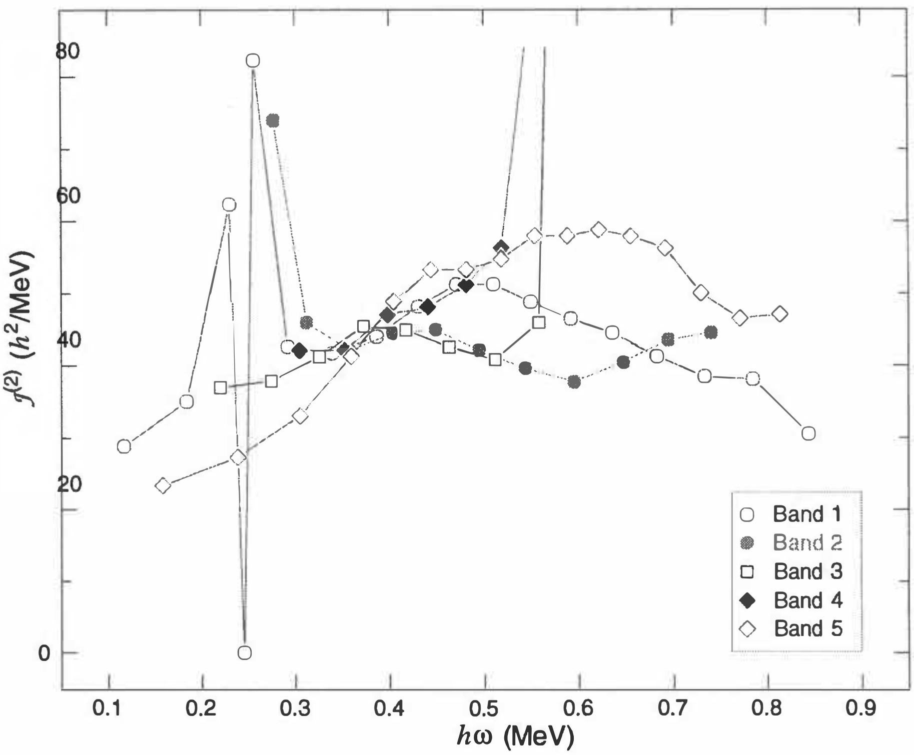

Figure 4.7: Dynamic moments of inertia for bands 1-5 in ^{123}La.

state band of ^{122}Ba. Thus, the E_pF_p crossing is blocked, which implies that band 3 is based on the [550]1/2 orbital (see Figs. 3.3 and 4.5). In addition, the large initial alignment ($\sim 5\hbar$), which is expected for a high-j, low-K state, supports this assignment. An alignment gain is observed over a frequency range $\hbar\omega_c = 0.35 - 0.68$ MeV (see Fig. 4.4(b)). Inspecting the dynamic moments of inertia ($\Im^{(2)}$), which can be a more sensitive indicator of interactions, for bands 1-5 in Fig. 4.7, one may observe a peak near $\hbar\omega_c \approx 0.45$ MeV for band 3. This is similar to the behavior found for bands 1 and 2; therefore, some of the alignment gain is associated with the EF crossing. However, band 3 experiences a second peak in the $\Im^{(2)}$ plot near 0.60 MeV that is not observed in bands 1 and 2. This is likely due to the F_pG_p crossing which is predicted to occur at $\hbar\omega_c \approx 0.61$ MeV by the CSM calculations in Fig. 4.5. This assignment is consistent with the observed F_pG_p crossing at $\hbar\omega_c \approx 0.64$ MeV for the [550]1/2 band in ^{125}La [40]. Therefore, the alignment gain observed in Fig. 4.4(b) for band 3 is a combination of the EF and F_pG_p crossings.

4.4.4 Band 4

The energy of the lowest state observed in band 4 (956.4 keV) makes a three-quasiparticle assignment unlikely as this is well below the rotational energy necessary to break a pair of nucleons in ^{123}La. However, the large initial alignment ($\sim$5 $\hbar$) seen in Fig. 4.4(b) for this sequence also discriminates against the $\pi(d_{5/2}/g_{7/2})$ and $\pi g_{9/2}$ configurations, as these orbitals cannot produce such large alignments. Indeed the only orbital near the Fermi surface that can produce such a large initial alignment is the $h_{11/2}$ state. Therefore, there are two possible scenarios for this structure. Band 4 may be the unfavored signature of band 3, in which case the spins would have to be decreased by one unit of $\hbar$ from those shown in Fig. 4.1. This would significantly move band 4 away from the yrast line which would not be consistent with the observed intensity. Instead, this sequence is suggested to be a γ-vibrational band based on the $\pi h_{11/2}$ configuration. Structures with similar decay patterns (*i.e.* with both $I \rightarrow I-2$ and $I \rightarrow I$ linking transitions) and excitation energies have been assigned this configuration in ^{123,125,127}Cs [50, 51, 52], ^{124,126}Ba [53, 54], ^{125}La [40], and ^{126}Ce [55]. Similar to the analogous structure in ^{125}La, the EF crossing occurs at a slightly lower frequency and has an even larger interaction strength than the pure $\pi h_{11/2}$ sequence (band 3).

4.4.5 Band 5

A three-quasiparticle assignment is possible for band 5 as the lowest state is observed at 1735.6 keV. The large initial alignment for this structure (see Fig. 4.4(b)) indicates at least one $h_{11/2}$ proton is involved in its configuration. It is possible that band 5 has a $\pi(d_{5/2}/g_{7/2})E_pF_p$ configuration, however, its alignment values are consistently $\sim$2 $\hbar$ lower than those of bands 1 and 2. One would expect alignment values similar to bands 1 and 2 if band 5 has this configuration. Since this is not the case, another scenario has been considered. One may notice that the alignment values of bands 4 and 5 are quite similar below 0.5 MeV, which may indicate the two have related structures. Thus, band 5 could possibly be the unfavored signature of the γ-vibrational band (band 4). Both signatures of the γ vibrational band have also been observed in the nearby nucleus ^{126}Ba [54] to high spin. Further discussions of bands 4 and 5 follow in the next section.

4.4.6 Band 6

The proton [404]9/2 orbital arising from the $g_{9/2}$ shell is the closest high-K state to the ^{123}La Fermi surface at prolate deformation. A strongly coupled structure is expected for this configuration, thus band 6 appears to be a good candidate for this excitation. The alignment plot of band 6, shown in Fig. 4.4(a), displays a crossing at $\hbar\omega_c \approx 0.34$ MeV. The crossing frequency and alignment gain appear to be consistent with those observed in the ground-state band of ^{122}Ba. It was concluded in Ref. [41] that the total alignment gain resulted from a combination of the E_pF_p and EF crossings. Thus, these same alignments are associated with the increase of $\sim 11\hbar$ observed for band 6 in Fig. 4.4(a). The reduced E_pF_p crossing frequency is not observed with the $\pi g_{9/2}$ band as blocking this up-sloping orbital only has a small effect on the pairing field, as discussed above.

In order to further confirm this configuration for band 6, the $B(M1)/B(E2)$ ratios were extracted and compared with theoretical predictions. Experimental $B(M1)/B(E2)$ ratios were determined from the observed γ-ray energies and branching ratios according to the standard formula [56]. The results of the $B(M1)/B(E2)$ analysis are plotted in Fig. 4.8 along with the theoretical calculations. The rotational model form of the $B(E2)$ transition strength [56] and an extended formalism [57] of the geometrical model from Dönau [58] and Frauendorf [59] for the $B(M1)$ strength were used to calculate theoretical $B(M1)/B(E2)$ ratios. An intrinsic quadrupole moment of $Q_0 = 4.58$ eb from the TRS prediction of $\beta_2 = 0.285$[1] for $\pi g_{9/2}$ was assumed. The collective gyromagnetic ratio was determined by $g_R = Z/A$ while g_K([404]9/2)=1.27 and g_K([550]1/2)=1.17 factors were determined from a Woods-Saxon potential calculation. Initial alignment values for the one-quasiparticle and three-quasiparticle configurations were obtained from Fig. 4.4(a). The $B(M1)/B(E2)$

[1]The TRS calculations predict a slightly larger deformation for this structure than the other sequences in ^{123}La.

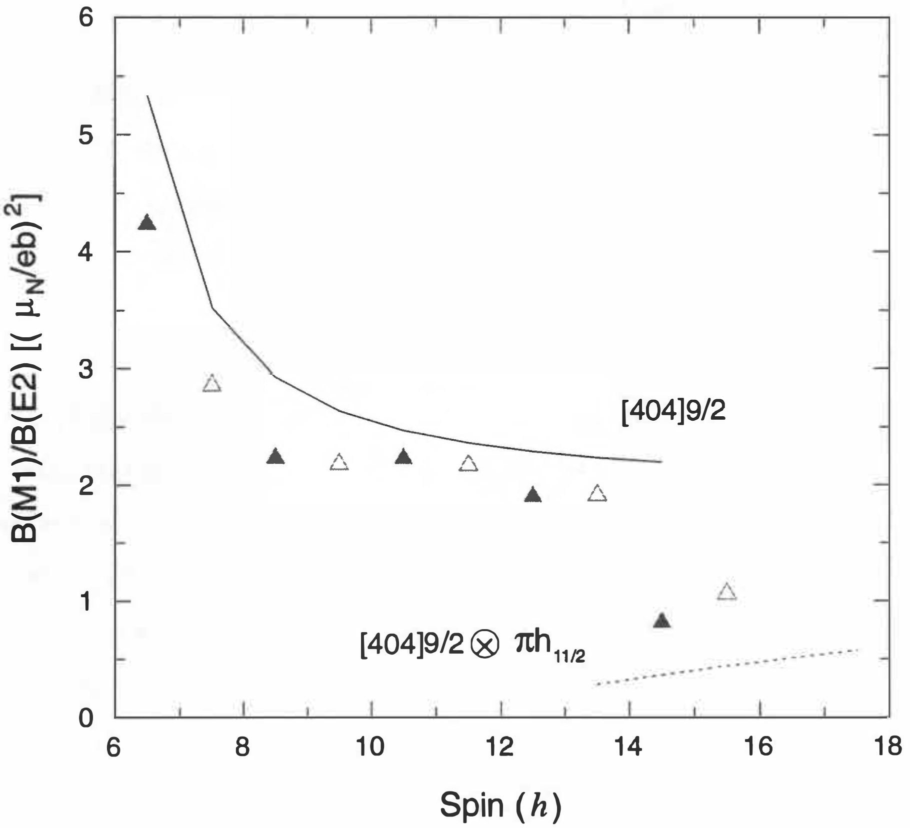

Figure 4.8: Experimental (symbols) and theoretical (lines) $B(M1)/B(E2)$ ratios for band 6 in ^{123}La. Parameters used for calculated values are discussed in the text.

ratios show good agreement between the experimental values and the theoretical calculations for the [404]9/2 orbital at lower spin although an overestimation is found in the calculated values, which may indicate a higher deformation than that predicted by the TRS calculations. A good fit of the experimental ratios is also achieved above $I = \frac{29}{2}$ with the theoretical values assuming a $\pi g_{9/2}\mathrm{E}_p\mathrm{F}_p$ assignment at higher spins.

4.5 The γ-vibrational Band

Rotational bands built on γ vibrations are observed in even-even and odd-A nuclei in the region. In the previous section, it was suggested that bands 4 and 5 may be γ vibrational bands coupled to the $\pi h_{11/2}$ configuration. Although this argument cannot be certain at this time, an effort to understand the characteristics of these two structures is addressed.

γ-vibrations are oscillations in which the nucleus retains its quadrupole deformation but oscillates about axial symmetry. In the neighboring Ba and Cs isotopes, γ-vibrational bands are observed and they are reported in a few La isotopes. As discussed in section 4.4, it is possible that bands 4 and 5 in ^{123}La are γ vibrational coupled to $\pi h_{11/2}$ due to their similar alignment behavior. Fig. 4.9 displays a plot of the excitation energy of the γ vibrational bandhead for various Ba and also La isotopes. We plot the energy of the 2^+_γ state for even-even Ba isotopes, and the energy of the $15/2^-_\gamma$ state relative to the bandhead energy of $\pi h_{11/2}$ for odd-A La nuclei. The γ band energy for the Ba isotopes is consistently around 900 keV. However, those for La increase with neutron number, different from the Ba trend. This difference in trends of the γ bandhead energies in La versus Ba may be related to the γ stiffness of the potential in each case. TRS calculations, illustrated in Fig. 4.10, indicate that for the yrast configuration the potential minima are slightly stiffer in the γ direction in odd-A La compared to Ba at $\omega = 0$ and $\omega = 0.062$ MeV. A stiffer potential in the γ variable should lead to a slightly higher γ band excitation energy for La nuclei compared to Ba, which is the trend exhibited in Fig. 4.9. This might explain that the proposed γ band excitation energy decreases as N decreases.

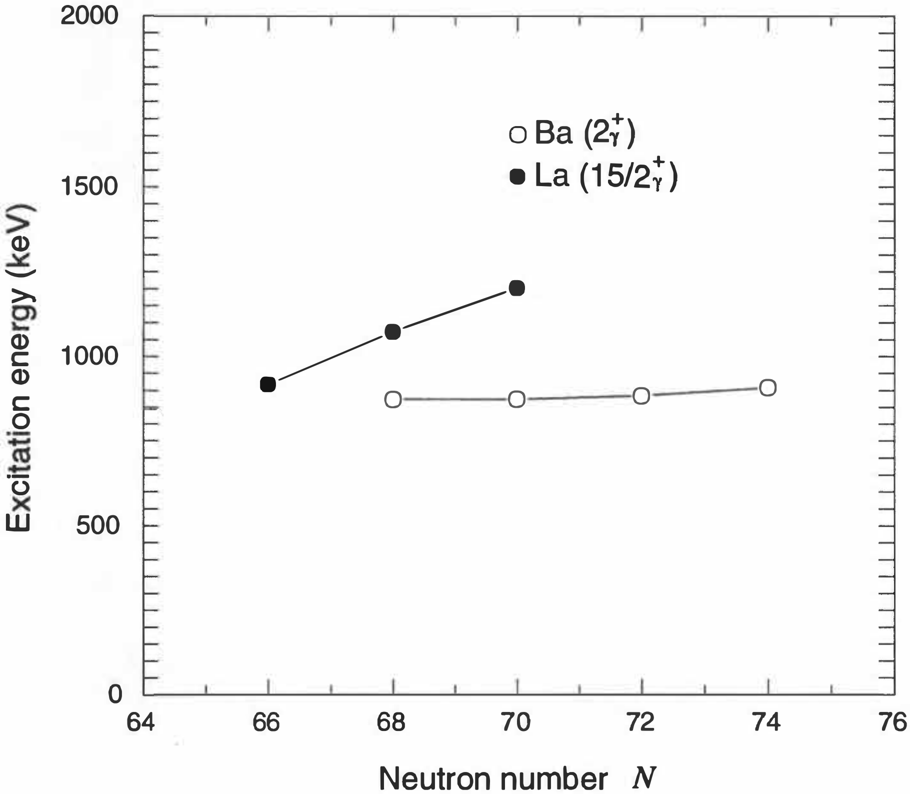

Figure 4.9: The plot of relative excitation energy between the γ-vibrational and ground-state bands. In even-even Ba, the energy of the 2^+_γ state is plotted. In odd-A La, the energy of the $15/2^-_\gamma$ state of the proposed γ band (band 4 in ^{123}La) is plotted.

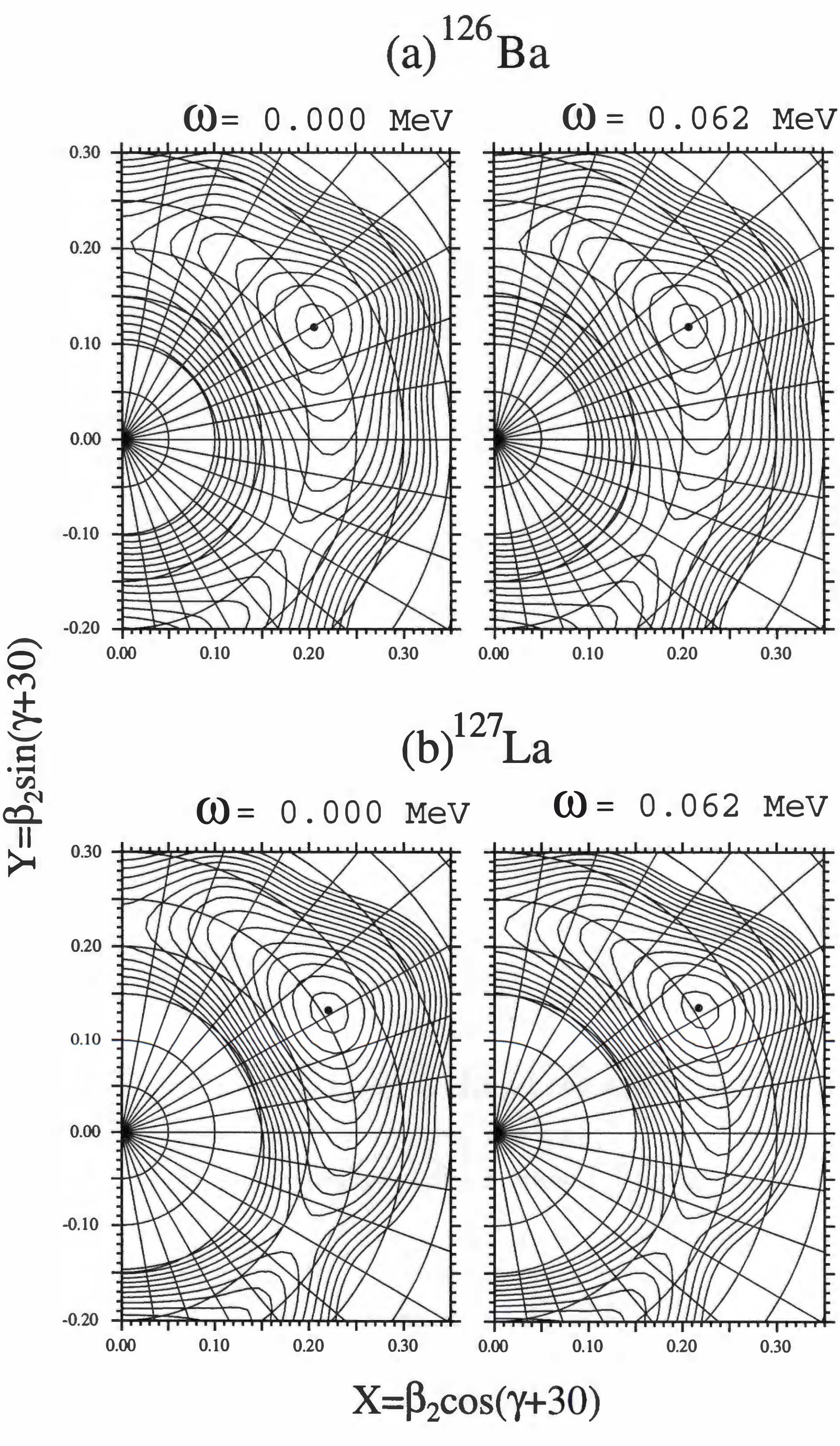

Figure 4.10: TRS calculations for the yrast configuration in ^{126}Ba and ^{127}La to display the softness of the nuclear surface.

CHAPTER 5

Discussion of Smooth Band Termination

Theoretical calculations [60] suggested that La isotopes could be good cases to study band termination in configurations with a few holes in the $N = 64$ core. In these configurations, the maximum spin value is $I = 40 - 50$. Recent work on heavier La nuclei [35, 36] provided the first experimental evidence that smooth band termination may indeed exist in ^{127,129}La. It is a general signature of smooth band termination that a minimum is formed in a plot of the excitation energy minus a rigid rotor energy $(E - E_{RLD})$ versus spin, which is a manifestation of limited angular momentum. Such evidence appears in Fig. 5.1 for the lowest $(\pi, \alpha) = (+, -\frac{1}{2})$ bands in ^{127,129}La [35, 36], and apparently for band 1 in ^{123}La. One observes for band 1 a constant value (~0.4 MeV) over the large spin range of $I \sim 10 - 33$ in the $E - E_{RLD}$ plot, followed by an increase in energy, similar to that found in the terminating bands of ^{127,129}La. Another indication of terminating states is that the dynamic moment of inertia $\Im^{(2)}$ decreases continuously as a function of rotational frequency and reaches the minimum value at the terminating point [27]. From our experimental data, a decline in $\Im^{(2)}$ is observed for band 1 in ^{123}La (see Fig. 4.7). Thus, at rotational frequencies above $\sim$ 0.65 MeV, the observed $\Im^{(2)}$ is considerably below the rigid rotor value, $\Im_{rig} \approx 45\hbar^2$/MeV.

In order to investigate whether the observed phenomena are the results of a smooth band termination, cranked Nilsson-Strutinsky (CNS) calculations were performed by Ingemar Ragnarsson similar to those in Refs. [35, 36]. The results of these calculations are shown together with experimental data of bands 1, 2, and 3 in Fig. 5.2. Since pairing is not included in the calculation, they are realistic only above the spin values of approximately $25\hbar$ but they can give a general description about

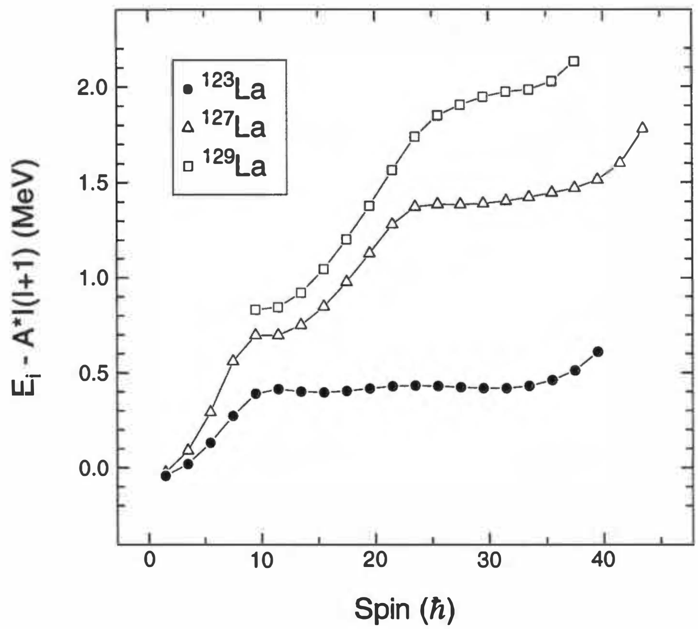

Figure 5.1: Excitation energy of states minus a rigid-rotor reference $(E - E_{RLD})$ versus spin for the lowest $(+, -\frac{1}{2})$ sequences in ^{123,127,129}La. The moment of inertia factor was scaled for each nucleus as described in the text.

the most important configurations also at lower spin. The configurations relative to the $^{114}_{50}Sn_{64}$ core were defined using the following nomenclature [27]

$$[p_1p_2, n] \equiv \pi(g_{9/2})^{-p_1}(h_{11/2})^{p_2}(g_{7/2}d_{5/2})^{Z-50+p_1-p_2}$$
$$\otimes \; \nu(h_{11/2})^{n}(g_{7/2}d_{5/2})^{-(64+n-N)},$$

i.e. p_1 is the number of proton holes in the $g_{9/2}$ orbitals, p_2 is the number of proton $h_{11/2}$ particles, and n is the numbers of neutrons in the $h_{11/2}$ orbitals. The parity of the configurations is determined by $\pi_{tot} = (-1)^{(p_2+n)}$.

The levels of band 1 are observed up to $I^{\pi} = \frac{79}{2}^{+}$. It is assigned to the [422]3/2 configuration at low-spin values, suggesting that this structure should have an even number of $h_{11/2}$ protons in the unpaired regime. Comparison of the calculations (see Fig. 5.2(a)) with the experimental values above $I \sim 30$ indicates that the [02,6] configuration best describes band 1. The studies of heavier La isotopes [36] reported that the [02,8] configuration was associated with the lower spin states of the [422]3/2 bands and was typically crossed by the [02,6] configuration, which leads to

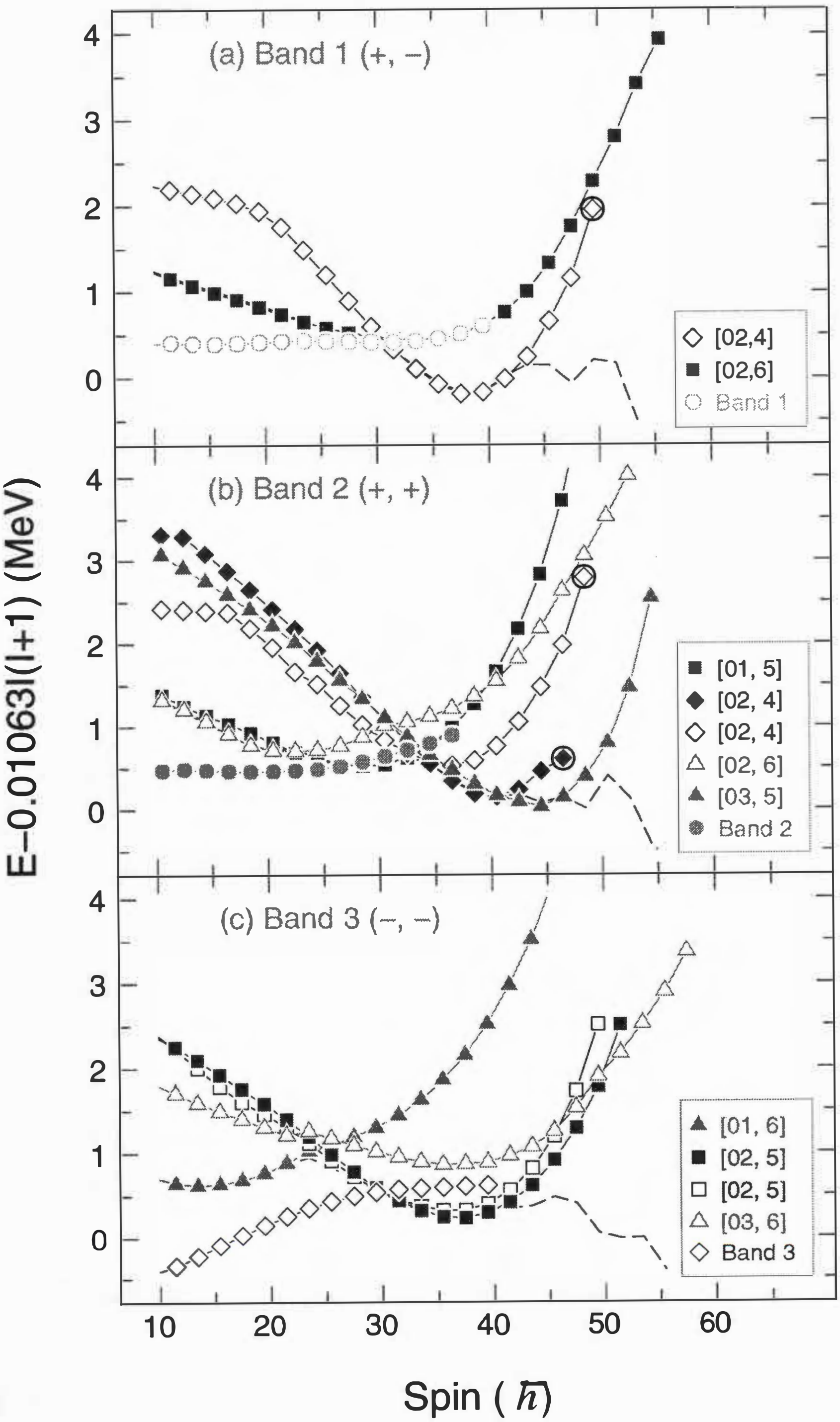

Figure 5.2: Comparison of experimental and theoretical $E - E_{RLD}$ energies. Cranked Nilsson-Strutinsky calculations produced the theoretical curves. Predicted terminating states are marked with a circle encompassing the symbol. The calculated yrast line for the given configuration is displayed as the dashed line in each panel.

the terminating state. It was found that the spin of this crossing was very close to the spin of the $h_{11/2}$ neutron alignment, as well. Following the analogous case for ^{123}La, the [02,4] configuration crosses the [02,6] configuration at $I \approx 30$ and terminates at $I = \frac{99}{2}$ (see Fig. 5.2(a)). However, the profile of band 1 does not correspond to that of the [02,4] configuration. In addition, the crossing at $I \approx 30$ does not agree with the experimentally observed band where it was suggested that the $h_{11/2}$ neutrons align gradually near $I = 20$. Since the neutron $h_{11/2}$ alignment in band 1 is occurring over a large range of frequency, it is difficult to observe this effect in the $E - E_{RLD}$ plot. Thus, band 1 appears to remain in the [02,6] configuration, contrary to the smooth band terminating effects seen in the heavier La nuclei. As an uncertainty of ~ 500 keV is assumed for these calculations, the [02,4] configuration may be higher in energy than that suggested in Fig. 5.2. Another possibility would be that the [02,4] band is indeed lower in energy in some spin range but not yet observed.

Band 2 was assigned a $\pi(g_{7/2}/d_{5/2})E_pF_p$ configuration suggesting that it has a [02,6] configuration at high spin although it is rather better described as a [01,5] configuration in Fig. 5.2(b). The irregular energies of the [02,6] (+,+) band is caused by a broad minimum extending over γ values, $|\gamma| \leq 20°$, with the minimum jumping from positive to negative γ with increasing spin (see Fig. 5.3). The true minimum would probably be described as some kind of linear combination of these 'two minima' resulting in a smoother energy. Once again, the calculated crossing of the [02,6] configuration by the [02,4] configurations is near $I = 30$, but the alignment plot in Fig. 4(a) indicates that the $h_{11/2}$ neutrons align gradually near $I = 20$. Thus, our experimental results indicate that bands 1 and 2 stay in [02,6] configurations contrary to those seen in ^{127,129}La.

For band 3, shown in Fig. 5.2(c), the calculations suggest that in the unpaired regime this band is associated with the [01,6] configuration at low spins and then [03,6] at higher spins. At $I \sim 25$, the [03,6] configuration crosses the [01,6] configuration, which reproduces the $h_{11/2}$ proton alignment qualitatively. Indeed, in Sec. IV above, this band was assigned as built on an odd $h_{11/2}$ proton at low spin values and with two additional protons aligned at high spin. With this interpretation, it must have at least three $h_{11/2}$ protons at high spin, i.e. the unpaired and paired

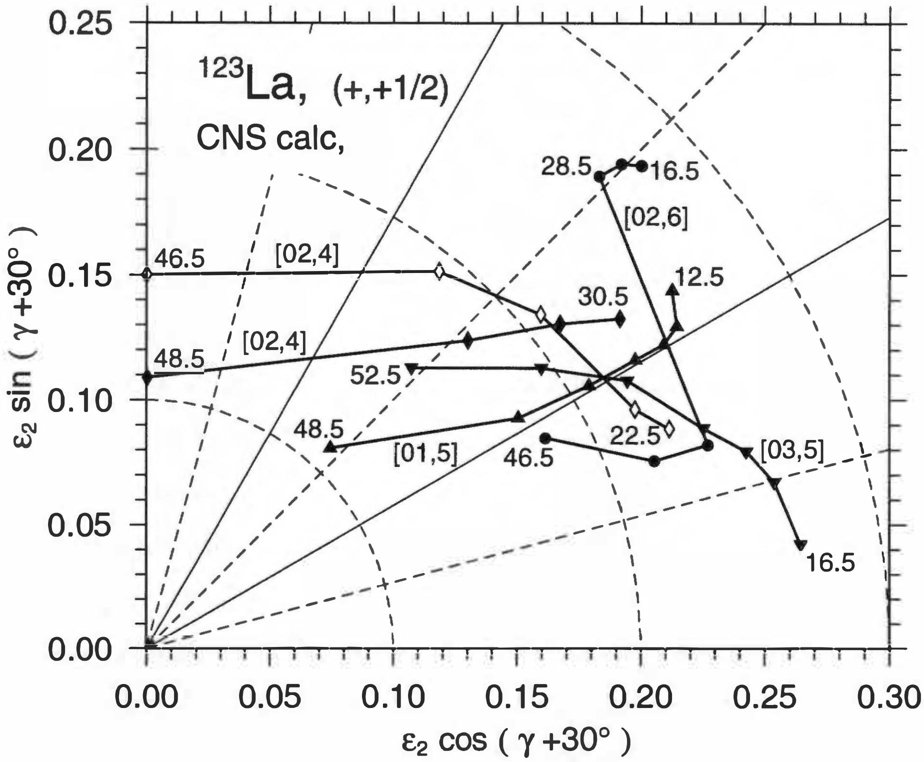

Figure 5.3: Calculated shape trajectories for the $(\pi, \alpha) = (+,+1/2)$ configurations of ^{123}La whose $E - E_{RLD}$ curves are drawn in Fig. 5.2(b). The equilibrium deformations for the different configurations are drawn in angular momentum steps of $6\hbar$. Both [02,4] configurations are seen to terminate at non-collective oblate shape, the [1,5] configuration is so soft towards the $\gamma = 60°$ axis for the $I = 48.5$ state that it becomes questionable if it should be considered to terminate or note while the "maximal spin" $I = 52.5$ state of the [3,5] configuration is much more clearly localized at γ values smaller than 30°. Finally, the [02,6] configuration never comes closer to the non-collective $\gamma = 60°$ axis than for $I = 46.5$. Note also the large spread in γ deformation for intermediate spin values which suggests some uncertainty in the analysis of the paired crossings where it was assumed that $\gamma = 0°$. The [02,6] configuration has an extended minimum in the γ direction, where the lowest energy is calculated for positive γ at low and intermediate spin values but at negative γ values in the high-spin region.

calculations give strong mutual support to the respective assignments. A difficulty with the present interpretation is that the unobserved [02,5] configuration is calculated 500-600 keV lower in energy than the [03,6] configuration. A further problem is that the signature $\alpha = 1/2$ [02,5] configuration is calculated at an even lower energy than the $\alpha = -1/2$ band shown in Fig. 5.2. Perhaps this latter configuration could be associated with band 5 in Fig. 4.1; however, the apparent observation of the EF crossing (see Fig. 4.4(b)) would seem to rule out any assignment with an odd number of $h_{11/2}$ neutrons.

The present calculations indicate that none of the bands in ^{123}La is observed to spin values close to termination. As seen in Fig. 5.2, it is only the [02,4] configurations which can be followed to termination in the CNS calculations but these bands are apparently not observed experimentally. The tendencies for different configurations to terminate is illustrated in Fig. 5.3 where the calculated shape trajectories of the (+,+1/2) bands are shown in the (ε, γ) plane. It is evident from Fig. 5.2(b) that the most favored termination occurs at $I = 46.5$ for a [02,4] configuration with the terminating state at $\varepsilon = 0.11$, $\gamma = 60°$. This non-collective state is built as the maximum-spin state in the configuration,

$$\pi[(h_{11/2})^2_{10}(g_{7/2}d_{5/2})^5_{11.5}]_{21.5}$$
$$\otimes\nu[(h_{11/2})^4_{16}(g_{7/2})^{-3}_{7.5}(d_{3/2})^1_{1.5}]_{25}$$

where the spin contribution from the different subshells is indicated by the subscripts. This specific state is also depicted in an e_i vs. m_i diagram [27] in Fig. 5.4. Note that in these terminating states, it is possible to distinguish between orbitals with their main components in the $g_{7/2}/d_{5/2}$ and in the $d_{3/2}$ (or perhaps more properly $d_{3/2}/s_{1/2}$) subshells, respectively. Indeed, although the $g_{7/2}$ and $d_{5/2}$ subshells are strongly mixed, we have shown the neutron holes as being only in the $g_{7/2}$ subshell as suggested from the labeling in Fig. 5.4. The [02,4] terminating states at $I = 49.5, 48.5$ are built with one more neutron excited from $d_{3/2}$ to $g_{7/2}/d_{5/2}$, i.e. where the neutron configuration is illustrated in Fig. 5.4. These two configurations differ in their occupation of the $g_{7/2}/d_{5/2}$ proton orbitals; either with three protons in signature $\alpha = -1/2$ and two in $\alpha = 1/2$ or three in $\alpha = 1/2$ and two in $\alpha = -1/2$. In the former

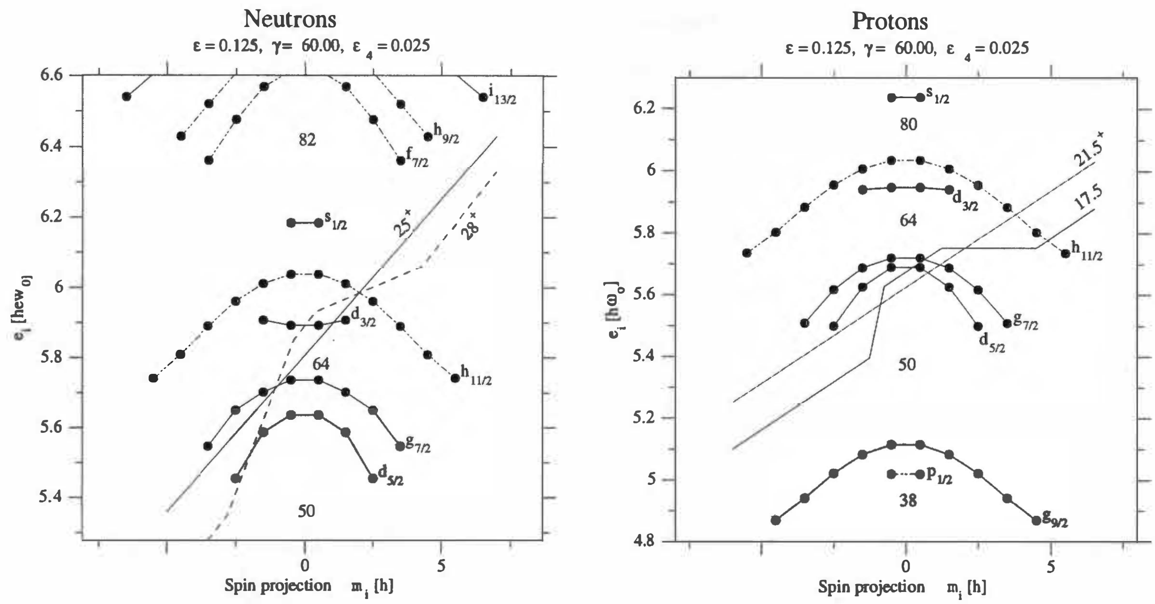

Figure 5.4: The single-particle energies at oblate shape e_i drawn vs. their spin projection on the symmetry axis, m_i. The deformation, $\varepsilon_2 = 0.125, \varepsilon_4 = 0.025$, is chosen as an average to be approximately correct for those valence space configurations which are calculated to terminate or come close to termination. Straight line sloping Fermi surfaces indicate the occupation of proton and neutron orbitals in the terminating $I = 46.5$ state of the [02,4] configuration. It is also shown that no straight line Fermi surface can be drawn for the $I = 28$, $(h_{11/2})^4$ neutron configuration of the [02,4] band which terminates at $I = 49.5$ or for the $I = 17.5$, $(h_{11/2})^1$ proton configuration of the [01,5] band which comes close to termination at $I = 48.5$. Note that the neutron Fermi surfaces come close to the high-m $(f_{7/2})$, $(h_{9/2})$ and $(i_{13/2})$ orbitals from the next major shell suggesting that aligned configurations with some of these orbitals occupied might become energetically competitive at spin values where the valence space configurations terminate

case, the maximum spin of these five particles is 11.5 [see Fig. 5.4(a)] while it is 10.5 in the latter case. Note that these two [02,4] bands are lowest in energy at low and intermediate spin values and it is only beyond $I \approx 35$ that the [02,4] configuration terminating at $I = 46.5$ becomes lower in energy. This configuration is special because it has a different number of $N = 4$ neutrons in the two signatures, namely seven $g_{7/2}$, $d_{5/2}$, $d_{3/2}$ neutrons with $\alpha = -1/2$ and five with $\alpha = 1/2$. Even though the maximum spin $I = 48.5$ state of the [01,5] configuration is not calculated to be axially symmetric, the energy minimum comes close to the non-collective $\gamma = 60°$-axis at this spin value. This becomes evident from the fact that the 'collective' minimum at $\varepsilon \approx 0.11, \gamma \approx 17°$ is very shallow being only 0.1 MeV lower than the lowest energy state along the $\gamma = 60°$ non-collective axis. The state in this 'non-collective minimum' can be considered as the maximum spin state in this configuration, namely $\pi[(h_{11/2})^1_{5.5}(g_{7/2}d_{5/2})^6_{12}]_{17.5} \otimes \nu[(h_{11/2})^5_{17.5}(g_{7/2}d_{5/2})^{-5}_{11.5}(d_{3/2})^2_2]_{31}$. If we try to form it in e_i vs. m_i diagrams, we note that it corresponds to sloping Fermi surfaces which are far from straight lines (as shown explicitly for the protons in Fig. 5.4). This is also what would be expected from the fact that this $I = 48.5$ state is calculated at a very high energy, see Fig. 5.2. The other configurations in Fig. 5.3 never comes close to termination. Thus, the minimum shown for the 'maximum spin' $I = 52.5$ state of the [03,5] configuration is approximately 0.5 MeV lower than the lowest energy at non-collective $\gamma = 60°$ deformation and the [02,6] configuration never come closer to $\gamma = 60°$ than for the $I = 46.5$ state shown in Fig. 5.3.

In the $I = 50 - 60$ range, bands of small collectivity are calculated to terminate as yrast. These states have one or several particles in the neutron orbitals emerging from the shells above the $N = 82$ gap (cf. Fig. 5.4). The lowest spin non-collective yrast state of this kind at $I = 101/2^-$ is built from three $h_{11/2}$ protons, four $h_{11/2}$ neutrons, and one $i_{13/2}$ neutron. It terminates at an oblate deformation of $\varepsilon \approx 0.25$.

CHAPTER 6

Summary

High-spin states have been investigated in the proton-rich nucleus ^{123}La. Three previously known sequences were extended to higher spins and three new structures were observed. Linking transitions were established between five of the bands for the first time, thus relative excitation energies are now known. Configurations were discussed for the bands based upon the observed alignment behavior. The possibility of the [422]3/2 structure displaying characteristics of smooth band termination was explored by comparing the data with cranked Nilsson-Strutinsky calculations. Although a minimum develops in the $E - E_{RLD}$ plot for the [422]3/2 band, the experimental data do not correspond with structures predicted to be near terminating states. Thus, it appears that none of the sequences in ^{123}La are consistent with predicted smooth band terminating structures. For further study, it is very important to experimentally populate much higher states to reach the predicted terminating state as this band is five transitions below the theoretical predictions. One way to approach this might be to introduce the next generation γ-ray arrays, such as GRETA (Gamma Ray Energy Tracking Array) for increasing the total detection efficiency by tracking events that would be rejected in Compton suppressed array. Based on more statistics, the comparisons between the theoretical calculations and experimental observables can be more effective to conclude the investigation of smooth band termination in the [422]1/2 band. Another attempt can be a measure of the lifetime for each state to see the decreasing collectivity with higher spins, but this will be very difficult to perform due to the weak intensity in the high-spin region. By scrutinizing alignments of these [422]3/2 bands in ^{123,125,127,129}La, a trend of the EF neutron $h_{11/2}$ crossing that occurs at successively lower frequencies can be developed with decreasing neutron number. The interaction strength for this crossing significantly decreases between ^{123}La and three heavier La nuclei. Two new bands observed in ^{123}La (bands 4 and 5) have rather high angular momentum but lie too low in energy to be three quasiparticle in nature. It is possible that these two bands correspond to a γ vibration coupled to the yrast $\pi h_{11/2}$ structure. The γ-band possibility for bands 4 and 5 was investigated by comparing to even-even Ba isotopes. The plot of relative excitation energy between the γ-vibrational and ground-state bands in Ba and La isotopes shows that those for La increase with neutron number while the Ba isotopes are consistently around 900 keV. A stiffer potential in the γ plane from TRS calculations for odd-A La compared to Ba could lead to a slightly higher γ band excitation energy for La. To confirm this qualitative explanation, a Coulomb excitation experiment would be possibly done to have more chance to observe the low-lying γ-vibrational band. Enhanced $B(E2)$ values of linking transitions to the yrast band is crucial to determine if our proposed γ-vibrational scenarios for bands 4 and 5 is correct.

BIBLIOGRAPHY

BIBLIOGRAPHY

[1] A. Galindo-Uribarri, Rev. Mex. Fis. **45**, 55 (1999).

[2] D.J. Hartley, A. Galindo-Uribarri, C. Baktash, M.P. Carpenter, M. Danchev, M. Devlin, C.J. Gross, R.V.F. Janssens, M. Lipoglavsek, E. Padilla, S.D. Paul, D.C. Radford, W. Reviol, L.L. Riedinger, D.G. Sarantites, D. Seweryniak, C.-H. Yu, and O. Zeidan, Phys. Rev. C **63**, 041301(R) (2001).

[3] O. Zeidan, D.J. Hartley, L.L. Riedinger, M. Danchev, W. Reviol, W.D. Weintraub, Jing-ye Zhang, A. Galindo-Uribarri, C.J. Gross, S.D. Paul, C. Baktash, M. Lipoglavsek, D.C. Radford, C.-H. Yu, D.G. Sarantites, M. Devlin, M.P. Carpenter, R.V.F. Janssens, D. Seweryniak, and E. Padilla, Phys. Rev. C **65**, 024303 (2002).

[4] D.J. Hartley, L.L. Riedinger, M. Danchev, W. Reviol, O. Zeidan, Jing-ye Zhang, A. Galindo-Uribarri, C.J. Gross, C. Baktash, M. Lipoglavsek, S.D. Paul, D.C. Radford, C.-H. Yu, D.G. Sarantites, M. Devlin, M.P. Carpenter, R.V.F. Janssens, D. Seweryniak, and E. Padilla, Phys. Rev. C **65**, 044329 (2002).

[5] O. Zeidan, D.J. Hartley, L.L. Riedinger, M. Danchev, W. Reviol, W.D. Weintraub, Y. Sun, Jing-ye Zhang, A. Galindo-Uribarri, S.D. Paul, D.G. Sarantites, M. Devlin, M.P. Carpenter, R.V.F. Janssens, and D. Seweryniak, Phys. Rev. C **66**, 044311 (2002).

[6] B. Cederwall, A. Johnson, B. Fant, S. Juutinen, P. Ahonen, S. Mitarai, J. Mukai, and J. Nyberg, Z. Phys. A **338**, 463 (1991).

[7] R. Wyss, F. Lidén, J. Nyberg, A. Johnson, D.J.G. Love, A.H. Nelson, D.W. Banes, J. Simpson, A. Kirwan, and R. Bengtsson, Nucl. Phys. **A503**, 244 (1989).

[8] F. Soramel, Phys. Rev. C **63**, 031304(R) (2001).

[9] G.L.D. Vretnar and P. Ring, Phys. Rev. Lett. **82**, 4595 (1999).

[10] W. Gelletly, "The Nuclear Whirligig," Nucl. Phys. News **2**, 1 (1992).

[11] O. Zeidan, "Spectroscopic Studies on High-Spin States in ^{128,129}Nd and ^{130}La," Ph.D. Thesis, University of Tennessee (December, 2002).

[12] D.C. Radford, Nucl. Instrum. Methods Phys. Res. A **361**, 297 (1995).

[13] R.Lucas, Europhys. News, No. 1, Vol 1 (2001).

[14] W.F. Mueller, Ph.D. thesis, University of Tennessee (1997).

[15] S.G. Nilsson, Dan. Mat. Fys. Medd. **29**, No. 16 (1955).

[16] S.G. Nilsson, C.F. Tsang, A. Sobiczewski, Z. Szymanski, S. Wycech, C. Gustafson, I.L. Lamm, P. Moller, and B. Nilsson, Nucl. Phys. **A131**, 1 (1969).

[17] N.A. Jelley, *Fundamental of Nucler Physics*, Cambridge University Press, Cambridge (1990).

[18] J. Bardeen, L.N. Cooper, and J.R. Schreifer, Phys. Rev. **108**, 1175 (1957).

[19] D.R. Inglis, Phys. Rev. **96**, 1059 (1954).

[20] D.R. Inglis, Phys. Rev. **103**, 1786 (1956).

[21] M.J.A. de Voigt, J. Dudek, and Z. Szymański, Rev. Mod. Phys. **55**, 949 (1983).

[22] S.G. Nilsson, I. Ragnarson, *Shapes and Shells in Nuclear Structure*, Cambridge University Press, Cambridge (1995).

[23] S. Åberg, H. Flocard, and W. Nazarewicz, Ann. Rev. Nucl. Part. Sci. **40**, 439 (1990).

[24] R.A. Sorensen, Rev. Mod. Phys. **45**, 353 (1973).

[25] P. Ring and P. Schuck, *The Nuclear Many-Body Problem*, Springer, Heidelberg, 1980.

[26] A. Bohr, B.R. Mottelson, and D. Pines, Phys. Rev. **110**, 936 (1958).

[27] A.V. Afanasjev, D.B. Fossan, G.J. Lane, and I. Ragnarsson, Phys. Rep. **322**, 1 (1999).

[28] T. Bengtsson and I. Ragnarsson, Phys. Scripta T5 (1983) 165.

[29] A.V. Afanasjev and I. Ragnarsson, Nucl. Phys. **A591**, 387 (1995).

[30] R. Wadsworth, R.M. Clark, J.A. Cameron, D.B. Fossan, I.M. Hibbert, V.P. Janzen, R. Krücken, G.J. Lane, I.Y. Lee, A.O. Macchiavelli, C.M. Parry, J.M. Sears, J.F. Smith, A.V. Afanasjev, and I. Ragnarsson, Phys. Rev. Lett. **80**, 1174 (1998).

[31] I. Ragnarsson, Slide report, Workshop on Nuclear Structure at moderate and high spin, Berkeley Oct. 13-16, 1986, LBL-22379, p. 50.

[32] F.G. Kondev, M A. Riley, R.V.F. Janssens, J. Simpson, A.V. Afanasjev, I. Ragnarsson, I. Ahmad, D.J. Blumenthal, T.B. Brown, M.P. Carpenter, P. Fallon, S.M. Fischer, G. Hackman, D.J. Hartley, C.A. Kalfas, T.L. Khoo, T. Lauritsen, W.C. Ma, D. Nisius, J.F. Sharpey-Schafer and P.G. Varmette, Phys. Lett. **B** 437 35 (1998).

[33] W.C. Ma, R.V.F. Janssens, T.L. Khoo, I. Ragnarsson, M.A. Riley, M.P. Carpenter, J.R. Terry, J.P. Zhang, I. Ahmad, P. Bhattacharyya, P.J. Daly, S.M. Fischer, J.H. Hamilton, T. Lauritsen, D.T. Nisius, A.V. Ramayya, R.K. Vadapalli, P.G. Varmette, J.W. Watson, C.T. Zhang and S.J. Zhu, Phys. Rev. C **65**, 034312 (2002).

[34] V.G. Soloviev, *Theory of Complex Nuclei*, Pergamon Press, Oxford (1976).

[35] C.M. Parry, R. Wadsworth, A.N. Wilson, A.J. Boston, P.J. Nolan, E.S. Paul, J.A. Sampson, A.T. Semple, C. Foin, J. Genevey, A. Gizon, J. Gizon, I. Ragnarsson, and B.G. Dong, Phys. Rev. C **61**, 021303(R) (2000).

[36] R. Wadsworth, E.S. Paul, A. Astier, D. Bazzacco, A.J. Boston, N. Buforn, C.J. Chiara, D.B. Fossan, C. Fox, J. Gizon, D.G. Jenkins, N.S. Kelsall, T. Koike, D.R. LaFosse, S. Lunardi, P.J. Nolan, B.M. Nyakó, C.M. Petrache, H. Scraggs, K. Starosta, J. Timár, A. Walker, A.N. Wilson, L. Zolnai, B.G. Dong, and I. Ragnarsson, Phys. Rev. C **62**, 034315 (2000).

[37] R.V.F. Janssens and F. Stephens, Nucl. Phys. News **6**, 9 (1996).

[38] D.G. Sarantites, P.-F. Hua, M. Devlin, L.G. Sobotka, J. Elson, J.T. Hood, D.R. LaFosse, J.E. Sarantites, and M.R. Maier, Nucl. Instrum. Methods Phys. Res. A **381**, 418 (1996).

[39] H. Iimura, M. Shibata, S.-I. Ichikawa, T. Sekine, M. Oshima, N. Shinohara, M. Miyachi, A. Osa, H. Yamamoto, and K. Kawade, J. Phys. Soc. Jpn. **60**, 3585 (1991).

[40] D.J. Hartley, L.L. Riedinger, H.Q. Jin, W. Reviol, B.H. Smith, A. Galindo-Uribarri, D.G. Sarantites, D.R. LaFosse, J.N. Wilson, and S.M. Mullins, Phys. Rev. C **60**, 014308 (1999).

[41] R. Wyss, A. Johnson, F. Lidén, J. Nyberg, D.J.G. Love, A.H. Nelson, D. Banes, A. Kirwan, and J. Simpson, in *Proceedings of XXV International Winter Meeting on Nuclear Physics, Bormio, 1987*, p. 542.

[42] C.M. Petrache, G. Lo Bianco, D. Bazzacco, Th. Kröll, S. Lunardi, R. Menegazzo, M. Nespolo, P. Pavan, C. Rossi Alvarez, G. de Angelis, E. Farnea, T. Martinez, N. Marginean, D.R. Napoli, and N. Blasi, Eur. Phys. J. A **12**, 135 (2001).

[43] S.M. Harris, Phys. Rev. **138**, B509 (1965).

[44] R. Bengtsson, S. Frauendorf, and F.-R. May, At. Data Nucl. Data Tables **35**, 15 (1986).

[45] R. Bengtsson and S. Frauendorf, Nucl. Phys. **A314**, 27 (1979); Nucl. Phys. **A327**, 139 (1979).

[46] R. Wyss, J. Nyberg, A. Johnson, R. Bengtsson, and W. Nazarewicz, Phys. Lett. **215B**, 211 (1988).

[47] K. Starosta, Ch. Droste, T. Morek, J. Srebrny, D.B. Fossan, D.R. LaFosse, H. Schnare, I. Thorslund, P. Vaska, M.P. Waring, R. Wyss, I.M. Hibbert, R. Wadsworth, K. Hauschild, C.W. Beausang, S.A. Forbes, P.J. Nolan, and E.S. Paul, Phys. Rev. C **53**, 137 (1996).

[48] F. Lidén, B. Cederwall, P. Ahonen, D.W. Banes, B. Fant, J. Gascon, L. Hildingsson, A. Johnson, S. Juutinen, A. Kirwan, D.J.G. Love, S. Mitarai, J. Mukai, A.H. Nelson, J. Nyberg, J. Simpson, and R. Wyss, Nucl. Phys. **A550**, 365 (1992).

[49] M. Diebel, Nucl. Phys. **A419**, 221 (1984).

[50] J.R. Hughes, D.B. Fossan, D.R. LaFosse, Y. Liang, P. Vaska, M.P. Waring, and J.-Y. Zhang, Phys. Rev. C **45**, 2177 (1992).

[51] J.R. Hughes, D.B. Fossan, D.R. LaFosse, Y. Liang, P. Vaska, and M.P. Waring, Phys. Rev. C **44**, 2390 (1991).

[52] Y. Liang, R. Ma, E.S. Paul, N. Xu, and D.B. Fossan, Phys. Rev. C **42**, 890 (1990).

[53] S. Pilotte, S. Flibotte, S. Monaro, N. Nadon, D. Prévost, P. Taras, H.R. Andrews, D. Horn, V.P. Janzen, D.C. Radford, D. Ward, J.K. Johansson, J.C. Waddington, T.E. Drake, A. Galindo-Uribarri, and R. Wyss, Nucl. Phys. **A514**, 545 (1990).

[54] D. Ward, V. P. Janzen, H. R. Andrews, D. C. Radford, G. C. Ball, D. Horn, J. C. Waddington, J. K. Johansson, F. Banville, J. Gascon, S. Monaro, N. Nadon, S. Pilotte, D. Prevost, P.Taras, and R. Wyss, Nucl. Phys. **A529**, 315 (1991).

[55] A.N. Wilson, R. Wadsworth, J.F. Smith, S.J. Freeman, M.J. Leddy, C.J. Chiara, D.B. Fossan, D.R. LaFosse, K. Starosta, M. Devlin, D.G. Sarantites, J.N. Wilson, M.P. Carpenter, C.N. Davids, R.V.F. Janssens, D. Seweryniak, and R. Wyss, Phys. Rev. C **63**, 054307 (2001).

[56] A. Bohr and B. R. Mottelson, *Nuclear Structure* Benjamin, New York, Vol. 2 (1975).

[57] V.P. Janzen, Z.-M. Liu, M.P. Carpenter, L.H. Courtney, H.-Q. Jin, A.J. Larabee, L.L. Riedinger, J.K. Johansson, D.G. Popescu, J.C. Waddington, S. Monaro, S. Pilotte, and F. Dönau, Phys. Rev. C **45**, 613 (1992).

[58] F. Dönau, Nucl. Phys. **A471**, 469 (1987).

[59] S. Frauendorf, Phys. Lett. **100B**, 219 (1981).

[60] A.V. Afanasjev and I. Ragnarsson, Nucl. Phys. **A608**, 176 (1996).

VITA

Hyo-In Park was born on June 9, 1976 in Seoul, Korea. She attended Colorado State University and received a Bachelor of Science in physics in May 1999. The following summer, she began her graduate studies in physics at the University of Tennessee, Knoxville. She expects to receive the Master of Science degree in May of 2003. After the completion of this work, she will continue her Ph.D. work at Vanderbilt University in the fall of 2003.